

**UNIVERSITÀ DEGLI STUDI DI PADOVA**

**DIPARTIMENTO DI BIOLOGIA**

**Corso di Laurea magistrale in Molecular Biology**



**TESI DI LAUREA**

**CSF1R inhibitors as a potential treatment for  
Duchenne Muscular Dystrophy: *in vivo*  
experiments in the *mdx* murine model**

**Relatore:** Prof. Libero Vitiello  
Dipartimento di Biologia

**Correlatore:** Prof. Dr. Fabio Rossi  
University of British Columbia, School of Biomedical Engineering,  
Department of Biomedical Sciences

**Laureanda:** Giulia Cordella

**ANNO ACCADEMICO 2022/2023**

## Abstract

Monocytes and tissue-resident macrophages are essential for responding to acute and chronic inflammatory conditions. Our research group has identified two populations of skeletal muscle-resident macrophages: a population of macrophages positive for lymphatic vessel endothelial receptor 1 (LYVE1) and T cell membrane protein 4 (TIM4), which self-renew and stay in the tissue, and a population of LYVE1-TIM4-macrophages, which are attracted as monocytes from the bloodstream upon injury. This study looks at the use of two CSF1R inhibitors, PLX3397 and PLX5622, as possible pharmacological intervention in the context of Duchenne Muscular Dystrophy (DMD). According to our findings, only PLX3397 efficiently reduces the number of tissue-resident macrophages and causes infiltrating macrophages to undergo metabolic reprogramming. We found that long-term treatment of *mdx* mice, the most commonly used animal model for DMD, with PLX3397 protected muscle against contraction-induced injury by altering the composition of muscle fibers from damage-sensitive glycolytic fibers to damage-resistant oxidative fibers. Given that CSF1R inhibitors are now undergoing clinical trials for chronic inflammatory illnesses, this study offers therapeutic approaches that appear promising in preventing muscle degeneration.

## Acknowledgments

This work would have not been possible without the encouragement and the support of Professor Fabio Rossi at the University of British Columbia, who patiently listened to me for hours discussing my crazy ideas and Professor Libero Vitiello from the University of Padua, for always being just a phone call away.

I want to extend my special thanks to Dr. Marine Theret, for feeding me amazing pastries and to Dr. Morten Ritso for the long days of numerous flow panels till the hours of dawn. A special thanks to both, for their valuable revision of my work, for their mentorship and guidance and for always finding the time to answer my “quick” questions.

Additionally, I would like to express my gratitude to Ian Coccimiglio for his support in the bioinformatic analysis and for being a great running coach and the rest of the Rossi Lab for always putting a smile on my face on the good days and bad days, putting up with my out of tune singing and for being a family away from home.

To my mum and my dad, thank you for driving me to be the best I can be. To my grandparents, thank you for already having the dinner planned the day I come home. To my sisters and my friends, thank you for always listening to me blabbing nerdy science facts and consoling me over my failed experiments.

## TABLE OF CONTENTS

Background.....	4
Duchenne Muscular Dystrophy (DMD).....	4
DMD pathophysiology.....	4
Inability to regenerate damaged muscle fibers.....	5
Accumulation of reactive oxygen species.....	5
Overloading of cytosolic calcium.....	6
Consequences of muscle damage.....	6
Tissue-resident macrophages.....	7
Fibroblast-macrophage interactions.....	8
CSF1 Receptor.....	8
Pexidartinib (PLX3397).....	9
PLX5622.....	10
Differences between PLX3397 and PLX5622.....	10
Aim of the Work.....	10
Results.....	12
Twenty-week CSF1R-inhibitor treatment increased body and muscle weight but did not affect muscle performance.....	12
Twenty-week CSF1R-inhibitor treatment changes proportions of circulating monocytes at resting state and after contraction-induced damage.....	15
Twenty-week CSF1R-inhibitor treatment changes proportions of skeletal muscle tissue-resident macrophages and fibro-adipogenic progenitors after contraction-induced damage.....	18
CSF1R inhibitors alter the metabolism of myofibers in mdx mice.....	21
Discussion.....	25
The effect of CSF1R inhibition on self-renewing tissue resident macrophages.....	26
Polarization of tissue-infiltrating macrophages via the CSF1/CSF1R and CSF2/CSF2R Axis.....	27
Metabolic reprogramming of muscle fibers in PLX3397-treated mdx mice.....	29
Conclusion.....	30
Materials and Methods.....	31
Bibliography.....	35

## BACKGROUND

### *Duchenne Muscular Dystrophy (DMD)*

Duchenne muscular dystrophy is a recessive, X-linked, severe genetic disorder characterized by progressive muscle wasting, atrophy and fibro-fatty tissue replacement. It affects about 1 in 5000 newborn males, which makes it the most common form of muscular dystrophy in children. The first symptoms manifest early during childhood and include frequent falls, difficulty walking, climbing stairs or running and a waddling gait. Most patients are wheelchair-bound around the age of 10 to 12 and often require ventilation assistance before reaching the age of 20. The majority of DMD patients pass away from cardiac or respiratory failure between the age of 20 and 40, even when provided with the best care. The disease is caused by the lack of dystrophin, a subsarcolemmal, structural protein which connects the cytoskeleton to the extracellular matrix via the dystrophin glycoprotein complex (DGC). Mutations in the DMD gene prevent the muscle isoform of dystrophin (Dp427m) from being produced. The large majority of mutations (~ 70%) are deletions, ranging from single exons to the whole gene; the remaining cases are due to either point mutations (~20%) or to duplications or more complex rearrangements. Additionally, epigenetic and post-translational modifications can lead to either decreased transcript synthesis or reduced capacity to bind with other proteins (Duan et al., 2021).

### *DMD pathophysiology*

Dystrophin and its binding partners form the dystrophin glycoprotein complex (DGC). Dystrophin and the DGC are essential for maintaining the stability of muscle membrane as well as the integrity of the cytoskeleton. The sarcolemma, actin microfilaments, intermediate filaments, microtubules, and other related structural proteins of the cytoskeleton, as well as channel, signaling, and scaffolding proteins, are among the structures with which dystrophin interacts both directly and indirectly. Dystrophin deficiency results in the disassembly of the DGC and in loss of the interaction between F-actin and the extracellular matrix. Disassembling the DGC has a variety of negative effects on muscle cell function because it plays crucial mechanical and signaling roles in preserving the structural integrity and contractile activity of muscle (Duan et al., 2021).

In healthy muscle, the sarcolemma is capable of absorbing the continuous mechanical stress caused by the repeated cycles of contraction and relaxation of the sarcomeres. The integrity of sarcolemma is maintained by the presence of a continuous network of proteins connecting the cytoskeleton with the extracellular matrix. In DMD, however, lack of dystrophin leads to a disarray of DGC, which in turns leaves the sarcolemma susceptible to contraction injury. Indeed, one of the biochemical hallmarks of DMD, as well as of its murine counterpart, is the drastic increase in the circulating levels of muscle's creatine kinase (CK), the sarcoplasmic enzyme which catalyzes the conversion

of creatine to phosphocreatine and adenosine diphosphate, indicating a ruptured sarcolemma (Paleo et al., 2022). Moreover, it has been found that muscles experiencing higher levels of stress demonstrate a higher degree of damage. As a result, muscles under constant repetitive strain like the diaphragm are affected earlier and more severely as the disease advances. Another indication linking mechanical stress with DMD pathogenesis comes from the observation that dystrophin expression begins early during development, although the appearance of symptoms coincide with the onset of walking. Similarly, in dystrophin-deficient *mdx* mice, the onset of muscular necrosis corresponds with increased cage activity, but limb immobilization halts the degeneration of muscles (Duan et al., 2021). The composition of the dystrophin glycoprotein complex (DGC) and the patterns of dystrophin expression further demonstrate the importance of muscular activity. In particular, there is a significant concentration of dystrophin in the muscle areas that undergo the most mechanical stress.

### ***Inability to regenerate damaged muscle fibers***

In human patients, the underlying cause of muscle atrophy, fibrosis, and adipogenesis in DMD is the inability to regenerate. According to some studies, the DGC is also directly involved in muscle regeneration (Duan et al., 2021). Satellite cells, also indicated as Muscle Stem Cells (MuSCs) are the adult stem cells of skeletal muscle and are situated between the muscle fiber's sarcolemma and basal lamina. In post-natal muscles they are normally quiescent but can be activated by fibers' damage, hence providing homeostatic muscle maintenance as well as muscle repair thanks to the production of committed myogenic progenitors via asymmetric division. Interestingly, activated MuSCs express the dystrophin protein, which appears to be crucial for controlling satellite cell polarity and thus, effective asymmetric division. Proper muscle regeneration depends on the balance between symmetric and asymmetric satellite cell division; alterations to this balance leads to unfavorable effects on muscle health. The polarized distribution of dystrophin upon activation of satellite cells limits the localization of the polarity effector kinase Par1b to the same surface, causing Pard3 to be driven to the opposite side of the cell (Dumont et al., 2015). Reduced numbers of asymmetric divisions significantly limit the formation of myogenic progenitors required for appropriate muscle regeneration in dystrophin-deficient *mdx* mice (Dumont et al., 2015). DGC disruption significantly reduces activated satellite cell myogenic commitment, hampering muscle regeneration. Failed regeneration can also result from indirect effects of matrix reorganization, epigenetic modifications, and chronic inflammation that are caused by the loss of dystrophin.

### ***Accumulation of reactive oxygen species***

The muscles of DMD patients and DMD animal models produce far more free radicals than healthy muscles. Reactive oxygen species (ROS) are produced, among the rest, by NADPH oxidase 2 (NOX2). NOX2 is activated by the microtubule-associated protein Rac1 with mechanical stretching of the muscle (Mosca et al., 2021). Due to the loss of

functional dystrophin in DMD, the microtubule structure thickens and becomes disorganized, which significantly accelerates the production of ROS by NOX2. Moreover, dystrophic muscle produces more free radicals due to the invasion of inflammatory cells and dysfunctional mitochondria. The production of free radicals in DMD muscle leads to recurring and permanent oxidative damage. Despite the fact that ROS have mainly been linked to damage, they also activate the transcription factor NRF2, which controls the activation of many antioxidant and anti-inflammatory target genes. NRF2 also modulates the NADPH oxidase enzyme activity, which has a central role in the pathophysiology of muscular dystrophies as a source of ROS (Mosca et al., 2021). Furthermore, oxidative stress affects dystrophic muscle more than it does healthy muscle. This is because glutathione, one of the most important antioxidants, is significantly decreased in dystrophic muscle (Almeida-Becerril et al., 2023). Despite mounting evidence connecting DMD's etiology to oxidative stress, traditional antioxidant therapy has not improved patient outcome.

### ***Overloading of cytosolic calcium***

Muscle from DMD patient and animal models, as well as patient-derived cell models have greater resting cytosolic calcium concentrations than healthy muscle (Duan et al., 2021). Metabolic abnormalities and mitochondrial-dependent necrosis are the outcome of mitochondrial dysfunction brought on by calcium excess. Additionally, sarcolemmal calcium enters through calcium channels, partially contributing to the excess in cytosolic calcium. Elevated sarcoplasmic calcium drives more release from sarcoplasmic stores, exacerbating the cycle. In dystrophic muscle, SERCA, which pumps sarcoplasmic calcium back into the SR, is downregulated, limiting the amount of excess so you have less chance of mopping up the excess calcium. In spite of this, patients with DMD have shown practically limited clinical improvement from calcium channel blockers, indicating that calcium overload may not be a viable therapeutic avenue to explore (Mareedu et al., 2021).

### ***Consequences of muscle damage***

As previously mentioned, the muscle damage caused by DGC instability results in dystrophic muscle with defective organelles and altered cellular components. Autophagy eliminates damaged organelles and protein aggregates from healthy muscles. In DMD, the potent autophagy inhibitor Akt becomes activated, leading to impaired autophagy (Duan et al., 2021). Consequent accumulation of damaged organelles and dysfunctional proteins eventually causes persistent inflammation and muscle fiber degeneration. DGC disintegration contributes to Akt activation, via the ROS-mediated stimulation of the Src/PI3 kinase pathway. Invading inflammatory cells sense and eliminate degenerated and injured muscle fibers. Macrophages and T lymphocytes make up the majority of the inflammatory cells that infiltrate the damaged muscle in young DMD patients (Li et al., 2022). In the early onset of inflammation, inducible NOS synthesis by pro-inflammatory macrophages facilitates muscle fibers lysis. In later

stages, pro-inflammatory macrophages polarize to anti-inflammatory macrophages that support fibrosis and regeneration (Theret et al., 2022). In dystrophic muscle, pro-resolving macrophages provide pro-fibrotic signals, rather than supporting myofibers regeneration. Apart from CD4+ helper T cells that produce inflammatory cytokines such as Interleukin-1 and 6, and Tumor Necrosis Factor-alpha (TNF- $\alpha$ ), to support other immune cells, there are also CD8+ cytotoxic T cells that induce apoptosis through a mechanism mediated by perforin (Osińska et al., 2014). Neutrophils, mast cells, and eosinophils also all contribute to the chronic inflammatory state observed in dystrophic muscle. In the early stages of the disease, regeneration helps to repair degenerated muscle. However, as the disease progresses, the chronic inflammatory environment of DMD muscle leads to the overexpression of TGF $\beta$ , which reduces myoblast fusion and ultimately results in the reduction of myogenic cell differentiation (Girardi et al., 2021). Additionally, muscle resident fibro-adipogenic progenitor (FAPs) clearance is impaired in dystrophic muscle of *mdx* mice, resulting in accumulation of matrix-producing cells and high levels of adipogenesis and fibrosis (Lemos et al., 2013).

### ***Tissue-resident macrophages***

During development, macrophages first appear and settle within particular tissues. Because of their capacity for self-renewal, these tissue-resident macrophages are independent of hematopoietic stem cells (HSC). Nonetheless, during postnatal tissue maturation, HSC-derived monocytes contribute to distinct macrophage populations in diverse tissues; in fact, many tissue-specific macrophages require ongoing monocyte replenishment until adulthood (Mass et al., 2023). For example, in the brain, the pool of resident macrophages (also called microglia) is established before birth and isn't sustained by blood monocytes. Conversely, in other organs like the skeletal muscle, there is both a population of resident macrophages that originates during embryonic development and another maintained by blood-derived monocytes (Mass et al., 2023; Duan et al., 2021). During homeostasis, resident macrophages in skeletal muscle primarily undertake tasks such as scavenging for debris and clearing necrotic or apoptotic cells. However, the precise role and significance of resident macrophages in responding to damage and subsequent tissue regeneration or degeneration remain unclear. While skeletal muscle can fully recover after acute injury, chronic damage, as seen in diseases like DMD, can lead to the development of fibrofatty infiltration in the muscle. In response to skeletal muscle injury, an intricate inflammatory process is triggered, involving the recruitment, proliferation, and activation of various hematopoietic cells, with macrophages predominantly derived from the bloodstream, playing a critical role in effective tissue regeneration (Arnold et al., 2007). Previous research shows that circulating monocytes infiltrate the muscle within a day of injury, giving rise to phagocytic macrophages expressing high lymphocyte antigen 6 complex locus C (Ly6C) and responsible for clearing necrotic fibers, cellular debris and stimulate myogenic cell proliferation. These macrophages then transition into pro-resolving LY6C<sup>Low</sup> cells, which promote myogenic cell differentiation, fusion and myofiber

growth (Theret et al., 2022). In contrast to the pro-resolving nature associated with resident macrophages, bone marrow-derived macrophages heighten inflammation at the injury site and worsen fibrosis. Notably, CCR2-deficient mice lacking monocytes have significantly reduced myofibers necrosis and fibrosis (Lazarov et al., 2023; Kamalika et al., 2014). These findings imply that targeting monocytes-derived and self-renewing macrophages could serve as a potential therapeutic strategy to mitigate inflammation and potentially enhance tissue repair processes in specific contexts.

### ***Fibroblast-macrophage interactions***

In various tissues, fibroblasts and macrophages are often closely associated, as shown by Uderhardt and colleagues through *in vivo* imaging (Uderhardt et al., 2019). Fibroblasts are an essential source of Colony-stimulating factor 1 (CSF1) for macrophages in stable states (Buechler et al., 2021). CSF1 can indicate expression of a transcriptional program specific to macrophages, boost survival, or act as a proliferative trigger (Hume et al., 2011). There are two different physiologically active forms of CSF1: the membrane-bound form and the secretory form ((Hume et al., 2011). Additionally, in fibrosis and inflammatory conditions, fibroblasts sustain the expression of *Csf1*, providing crucial signals to resident or infiltrating macrophages within fibrotic lesions (Buechler et al., 2021). Notably, activated macrophages stimulate the production of CSF1 protein from fibroblasts *in vitro* (Meziani et al., 2018). In fibrotic conditions, macrophages can provide direct signals to fibroblasts to elicit their proliferation, such as Platelet Derived Growth Factors (PDGFs), and provide signals such as TGF $\beta$ 1, IL-1 $\beta$ , IL-6, and granulins, which can directly activate fibroblasts (Theret et al., 2022). Furthermore, activated fibroblasts generate the macrophage chemoattractant CCL2, indicating their capability to attract monocytes or macrophages to sites of injury or fibrosis (Meziani et al., 2018). Macrophage depletion at the onset of fibrosis constrained the extent of fibrotic injury in skeletal muscle, whereas their loss during fibrotic resolution prolonged fibrosis (Wang et al., 2022). Macrophages can influence fibroblasts both directly through cell-cell interactions and indirectly through signals involving other cell types and the extracellular environment (Buechler et al., 2021). Moreover, fibroblasts and macrophages can interact indirectly through the extracellular matrix (ECM): fibroblasts deposit and organize, while macrophages degrade it (Buechler et al., 2021).

### ***CSF1 Receptor***

CSF1 serves a crucial role in the recruitment of monocytes from peripheral blood, their differentiation into macrophages, and the polarization of these macrophages toward an anti-inflammatory phenotype (Theret et al., 2022). All of this is done through the binding to the receptor, CSF1R. The signaling cascade initiated by CSF1/CSF1R is fundamental for the differentiation and survival of macrophages (Buechler et al., 2021). CSF1 is constitutively secreted by a wide variety of cell types and tissues as three isoforms, two of which are found in the blood. CSF1R, a receptor tyrosine kinase,

undergoes oligomerization and autophosphorylation upon binding to its ligands, CSF1, or IL-34 (Theret et al., 2022). Studies on mice lacking functional CSF1 ligands or receptors have shown a notable decrease in macrophage populations (Ries et al., 2015). Consequently, the inhibition of the CSF1/CSF1R axis to target tissue-resident macrophages has garnered significant interest in recent times. Several ongoing or recently completed clinical studies are exploring the manipulation of this pathway in the context of cancer research (Ries et al., 2015). Injections of recombinant CSF1 into mice induce proliferation of most tissue-resident macrophages, followed by a gradual return of macrophage density to homeostatic levels upon treatment cessation. Studies of individual CSF1 isoforms in mice show that the membrane-bound isoforms can fully restore macrophage densities in CSF1-deficient mice throughout many tissues but not in the liver, adrenal gland, spleen or peritoneal cavity, suggesting that the membrane bound isoform might be responsible for niche maintenance. Mice lacking CSF1 are deficient in most tissue-resident macrophages. This makes sense due the fact that IL-34 is produced mainly by neurons and keratinocytes (Fujiwara et al., 2019). Both CSF1 and IL-34 signal to macrophages via the CSF1R.

### ***Pexidartinib (PLX3397)***

Pexidartinib (PLX3397) is a selective tyrosine kinase inhibitor that can be ingested orally and can cross the blood-brain barrier (BBB). It primarily targets macrophage colony stimulating factor-1 receptor (CSF-1R), although it also inhibits FLT3 and c-Kit, two receptors with similar structure. Early-stage clinical trials on humans had examined the potential of PLX3397 as a potential therapeutic for a variety of tumors. Clinical trials have assessed the safety, tolerability, and efficacy of PLX3397 in patients with a variety of cancer types, such as glioblastoma, melanoma, and different solid tumors (Ries et al., 2015). C-Kit (also known as CD117), encodes for a glycosyl-phosphatidylinositol (GPI)-linked cell surface glycoprotein, responsible for neutrophil activation. Mutations in this gene cause myeloproliferative disorders. An example is thrombocytopenia, a disease that leads to an excessive amount of platelets being produced by the bone marrow, which affects blood clotting and increases risks of thrombosis. FLT3 (also known as CD135), is mostly expressed on the surface of bone marrow-derived hematopoietic progenitor cells. Hematopoietic progenitors depend on CD135 for both self-renewal and maintenance. It also helps these cells differentiate into distinct lymphoid and myeloid lineages. Acute myeloid leukemia and lymphoblastic leukemia are exacerbated by FLT3 mutations, which cause uncontrolled cell survival and replication (Ries et al., 2015). PLX3397 interacts with the juxtamembrane area of CSF1R. Pexidartinib has the ability to either deplete macrophages and microglia or alter their function and possibly polarization, depending on the dosage (Fujiwara et al., 2021). This study shows that in contrast to tumors treated with vehicle, tumor-associated macrophages (TAM) from PLX3397-treated tumors were polarized toward an inflammatory phenotype. Furthermore, treatment with PLX3397 resulted in an increase in CD8<sup>+</sup> T-cell infiltration while decreasing CD4<sup>+</sup> T-cell infiltration. *In*

*in vitro* treatment of PLX3397 suppressed pERK1/2 stimulation by CSF1, and reduced anti-inflammatory polarization, survival, and chemotaxis in BMDMs (Fujiwara et al., 2019). Pexidartinib has mostly been studied for treating different forms of cancer, currently as a complement therapy treating Tenosynovial giant cell tumors, but has mainly failed as a monotherapy for other cancer types.

### ***PLX5622***

PLX5622 is a highly-specific CSF1R inhibitor that can cross the BBB very efficiently. In comparison to PLX3397, the use of PLX5622 in humans has not yet been approved. Preclinical research has indicated that this medication may be useful in treating neuroinflammatory and neurodegenerative diseases (King Nicholas et al., 2023). Through research in animal models, PLX5622 has shown promise in reducing the number of activated microglia and reducing neuroinflammatory reactions. PLX5622 permits the prolonged and targeted degradation of microglial cells in the early stages of disease progression. This chemical exhibits stronger depletion efficiency than previously developed CSF-1R inhibitors such as PLX3397, with an additional 20-fold selectivity for CSF-1R over c-Kit and FLT3. This compound was specifically designed to improve the penetration of CSF1R inhibitors through the BBB. Previous studies have indicated that PLX5622 is a valuable chemical to study the dynamics of microglia. According to Spangerberg et al., >95% of microglia were depleted from mouse brains both before and during the development of Alzheimer's disease through a treatment lasting up to 6 months (Spangenberg et al. 2019). Thus, it is possible for microglia to be consistently and selectively eliminated both before and during the pathological development of Alzheimer. The long-term reduction of microglia induced by PLX5622 is very stable and specific to the microglial cell populations.

### ***Differences between PLX3397 and PLX5622***

The amino acid Gly-795 is a gate-keeper to the interior allosteric pocket of CSF1R. PLX5622 was designed to specifically access the space between Gly-795 and CSF1R by adding 2-fluoro substitution on the middle pyridine ring. This change assures that PLX5622 does not competitively inhibit c-Kit and FLT3, as both have a bulkier structure that cannot be accessed by the compound. Furthermore, after the juxtamembrane domain is displaced, the terminal pyridine group of PLX5622 stabilizes the allosteric pocket of CSF1R (King Nicholas et al., 2023). The middle pyridine ring's orientation and position when PLX5622 binds to c-Kit or FLT3 result in steric collision with the gate-keeper cysteine, impairing the terminal pyridine moiety's ideal fit. PLX5622 has lower molecular weight, higher lipophilicity and better cell permeability, all factors that increase its ability to cross the BBB (~20%, compared to ~5% for PLX3397) (King Nicholas et al., 2023).

### ***Aim of the Work***

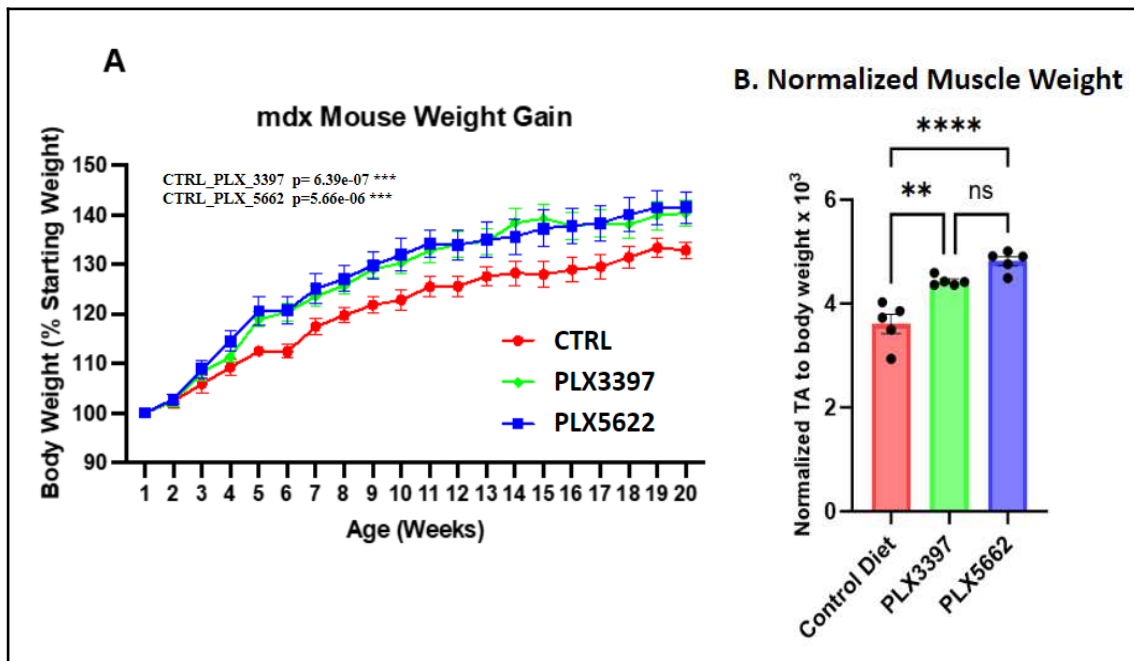
The aim of this study is to investigate CSF1R inhibitors as potential therapeutic strategies to target muscle degeneration in the *mdx* murine model of DMD. We are exploring a long-term treatment of 20 weeks in parallel with two different inhibitors: PLX3397 and PLX5622. Throughout the course of the 20 weeks, functional studies tracking muscle strength and endurance are used to monitor therapy outcomes. Additionally, we investigate the dynamics of the immune cell population in the blood using flow cytometry, both before and after exercise to cause eccentric stress in the muscle's limbs, and we track any potential mechanisms of degeneration and regeneration across the three conditions. After administering CSF1R inhibitors for 20 weeks, we take blood and skeletal muscle samples. We perform additional flow cytometry analysis to examine the effect of CSF1R inhibition on blood-circulating monocytes, infiltrating macrophages and self-renewing tissue resident macrophages. We use histology to identify potential metabolic reprogramming of muscle fibers in limb skeletal muscle following contraction-induced damage. This work presents treatment strategies that are promising for preventing muscle degeneration in DMD.

### **RESULTS**

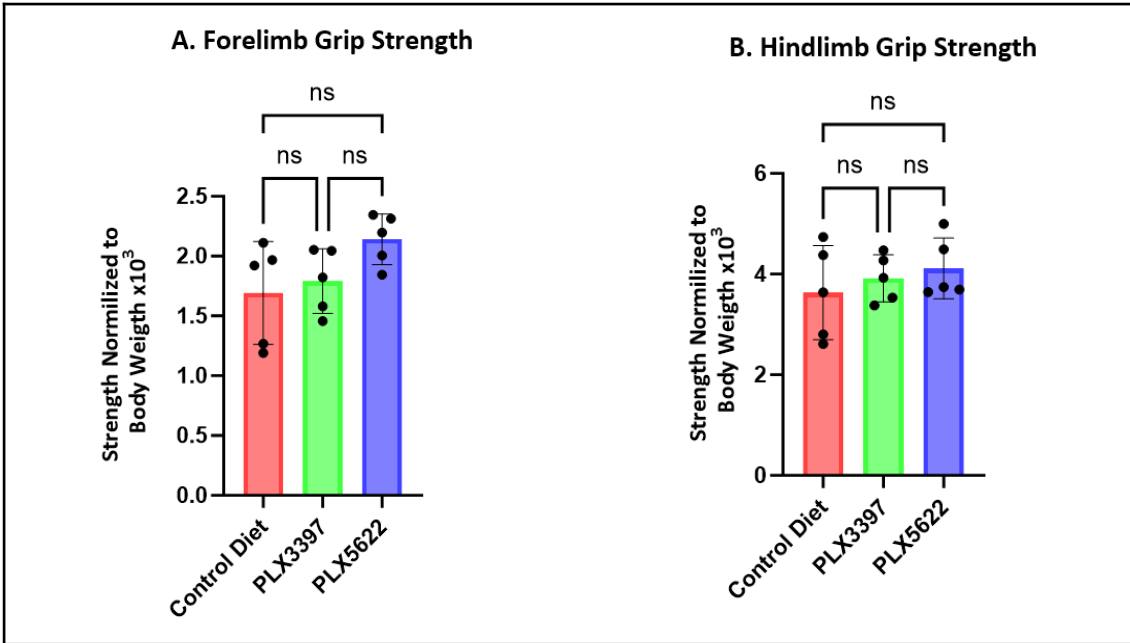
#### ***Twenty-week CSF1R-inhibitor treatment increased body and muscle weight but did not affect muscle performance***

In order to determine the therapeutic potential of CSF1R inhibitors in muscular dystrophy we investigated the outcome of long-term treatment in *mdx* mice. While *mdx* mice undergo significant necrosis in their skeletal muscles between 4 and 6 weeks of neonatal life, onset of muscle fibrosis does not happen until later in adulthood. Therefore, we began administering therapy to five *mdx* mice per condition at 8 weeks of age in order to examine the impact of CSF1R inhibitors in a chronic fibrotic setting, as is seen in DMD patients. Since diaphragm and tibialis anterior (TA) muscle deterioration become apparent around 6 months of age, treating dystrophic *mdx* mice at an earlier age enables us to test the preventative effects of our proposed treatment method. Mice were treated for 20 weeks, and sacrificed at 28 weeks of age. The control chow, PLX3397 and PLX5622 diets, were given to three groups of mice *ad libitum*. Body weight of the mice was monitored weekly throughout the 20 treatment course. ANCOVA analysis showed a significant difference in weight at multiple time-points when comparing each of the PLX compounds to the control diet group, but not between the two inhibitors. Both groups of mice treated with the CSF1R inhibitors had a significant weight gain in comparison to control diet mice (Figure 1A). Similarly, we observed a significant increase in TA muscle weight (Figure 1B). We also tested functional abilities at the end of treatment, at week 18, 19 and 20. We observed a trend towards improved function by grip strength, for the hind limbs (Figure 2B) and horizontal treadmill exercise performance. The data reported shows result from a single session with total distance, work and power averaged per condition (Figure 3A). In

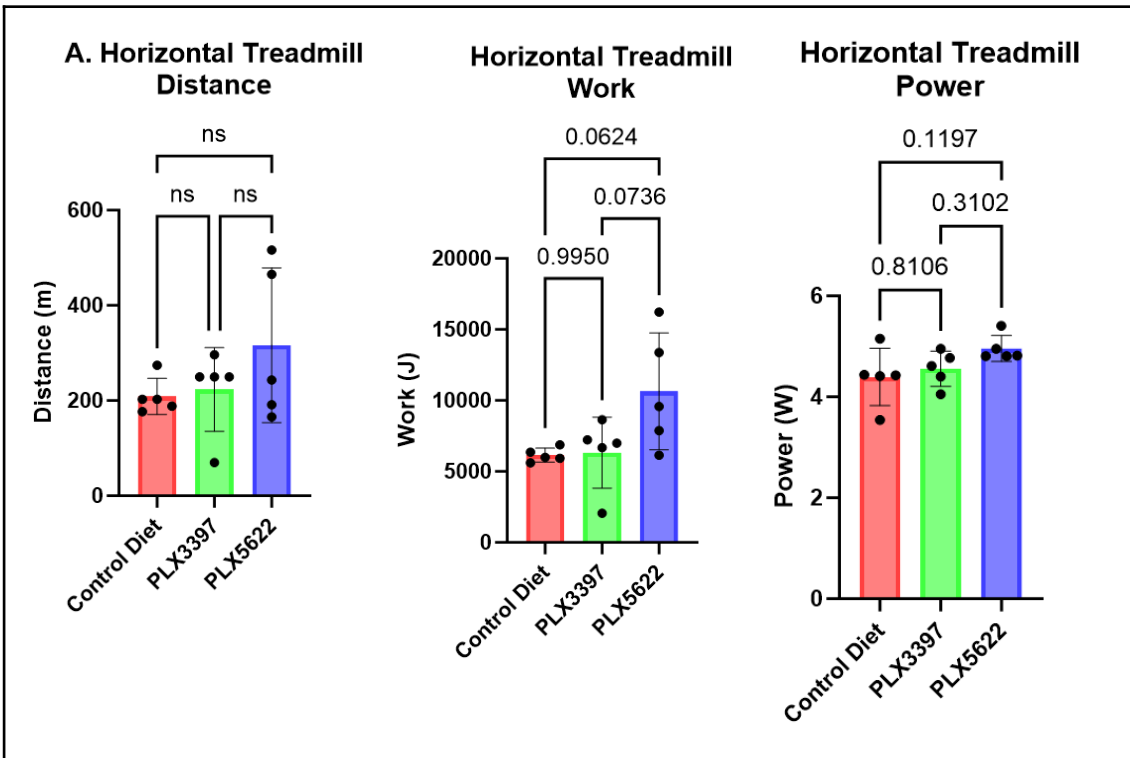
order to investigate if CSF1R inhibition further protects dystrophic muscle in vivo, we subjected both treated and control *mdx* mice to an exercise session on a moderately intense downhill treadmill. Eighty percent of the workout session was completed by all of the mice. We evaluated the rodents' performance in both declining and horizontal modes on both treadmill routines. Treadmill exercise performance on the horizontal (Figure 3A) and downhill (Figure 3B) planes showed the same trend for both inhibitors, suggesting that the mice treated with the inhibitors have greater endurance and resistance to eccentric stress. This trend is also evident when adjusting the distance to body weight by calculating the work performed. When considering the power and taking time into account, the trend becomes less apparent. Only mice in the PLX5622 group showed significantly improved work and power during a downhill treadmill exercise (Figure 3B).



**Figure 1.** (A) Recorded muscle weight represented as percentage body weight increase compared to starting weight. ANCOVA with post-hoc Tukey's multiple comparison test (B) Tibialis anterior (TA) muscle weight normalized to body weight was significantly increased in mice treated with both inhibitors. One-way ANOVA with post-hoc Tukey's multiple comparison test (\*\*p<0.001; \*\*\*\*p<0.0001).



**Figure 2.** (A) Forelimb grip strength does not show a significant improvement with CSF1Ri treatment. (B) Hindlimb grip strength does not show a significant improvement with CSF1Ri treatment. Experiment was done on week 19 of treatment. One-way ANOVA with post-hoc Tukey's multiple comparison test. ( $p=0.1$ )



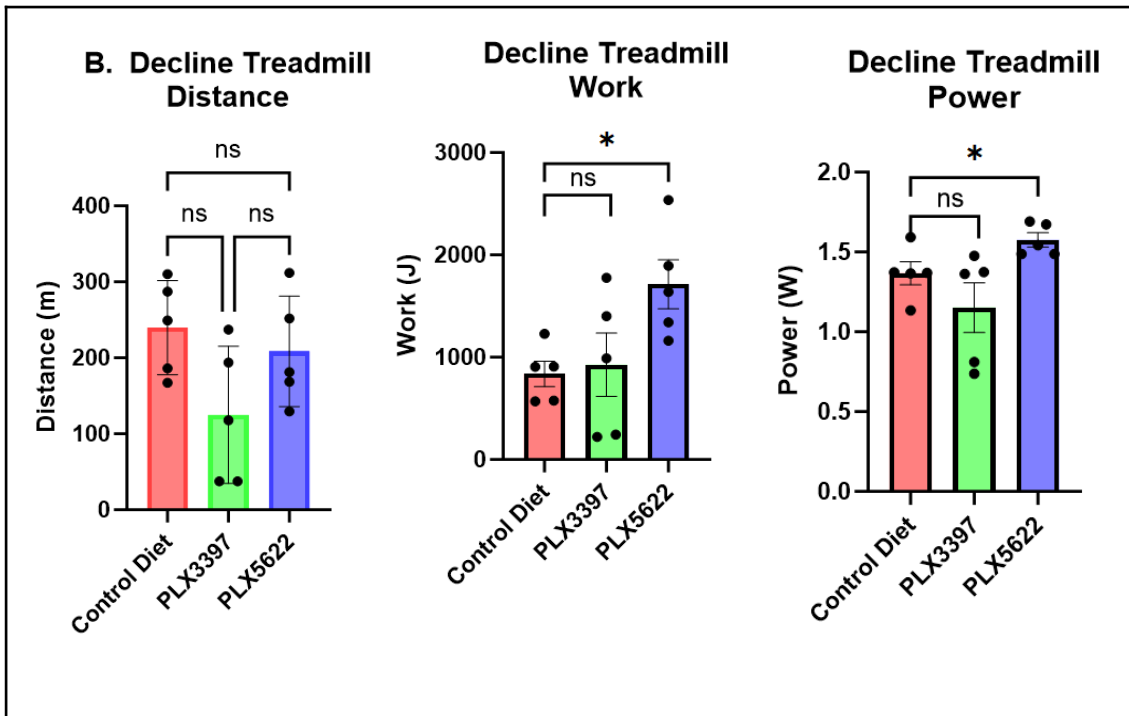


**Figure 3.** (A) Horizontal treadmill exercise shows a trend toward increased distance and time spent running on the treadmill. One-way ANOVA with post-hoc Tukey's multiple comparison test. (B) Mice in the PLX5622 group showed significantly improved work and power during a downhill treadmill exercise. Error bars represent the standard error of the mean. One-way ANOVA with post-hoc Tukey's multiple comparison test for distance and Unpaired T-test for work and power (\* $p < 0.05$ ).

***Twenty-week CSF1R-inhibitor treatment changes proportions of circulating monocytes at resting state and after contraction-induced damage.***

As it has been previously shown that CSF1 inhibitors affect circulating immune cells and their infiltration into tissues (Babaeijandaghi et al., 2022), we conducted blood analysis to study immune cell dynamics both before and after treadmill activity in decline by using flow cytometry. Blood samples were collected the same day before and after induction of eccentric damage by exercise and we analyzed proportions of neutrophils, eosinophils and monocytes, as well as T and B cells. Our findings show that there is no significant difference in percentage of circulating monocytes at resting state, however mice treated with both CSF1R inhibitors have a significantly higher percentage of Ly6C<sup>+</sup> monocytes (Figure 4A). After exercise-induced damage, there is a significant decrease in proportion of circulating monocytes in the *mdx* mice treated with both CSF1R inhibitors with the treadmill exercise in decline. Additionally, only mice treated with PLX3397 show a significant increase in percentage of Ly6C<sup>+</sup> out of the total number of monocytes after eccentric damage (Figure 4B). All experimental groups, regardless of the therapeutic strategy, showed a significant decrease in the amount of circulating eosinophils following exercise (Figure 5A). Exercise lowered B

cells and Ly6C<sup>+</sup> patrolling monocytes under any condition (Figure 5A). However, when comparing the two CSF1R inhibitors, PLX5622-treated mice had significantly higher eosinophil counts than either the PLX3397 or the control diet group as a response to eccentric damage while no difference was visible beforehand (Figure 5B). Other immune cell populations were not affected by inhibitions of CSF1R.

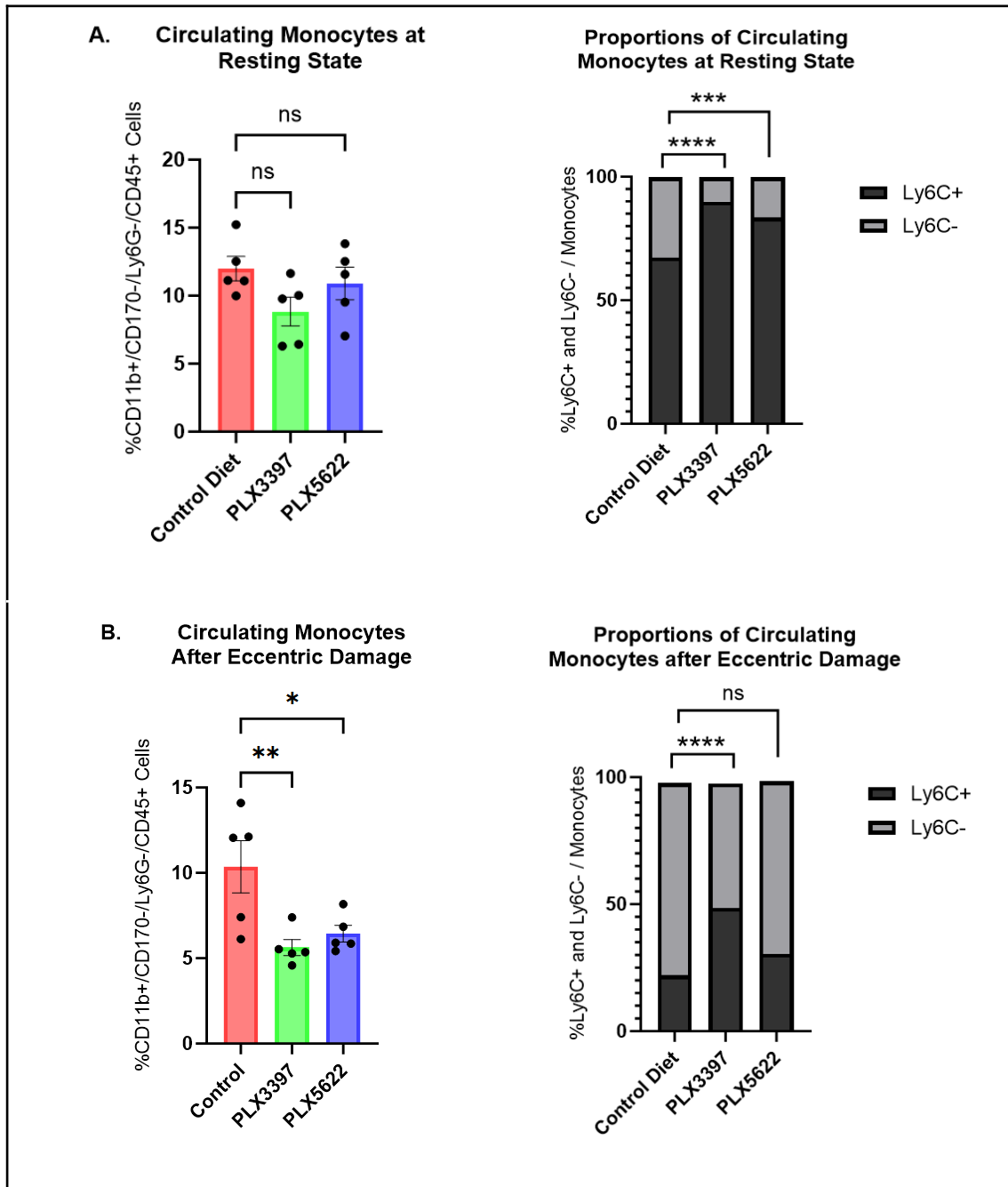


**Figure 4.** (A) Difference in percentage of circulating monocytes at resting state measured by flow cytometry. (B) Proportion of circulating monocytes after treadmill exercise in decline. Percentage of monocytes is calculated out of the total viable CD45<sup>+</sup> cells. The proportion of Ly6C<sup>+</sup> and Ly6C<sup>-</sup> monocytes is calculated out of the total number of monocytes. Two-way Anova with post-hoc Tukey's multiple

comparison test, for both A and B \*\*\*p<0.001; \*\*\*\*p<0.0001.

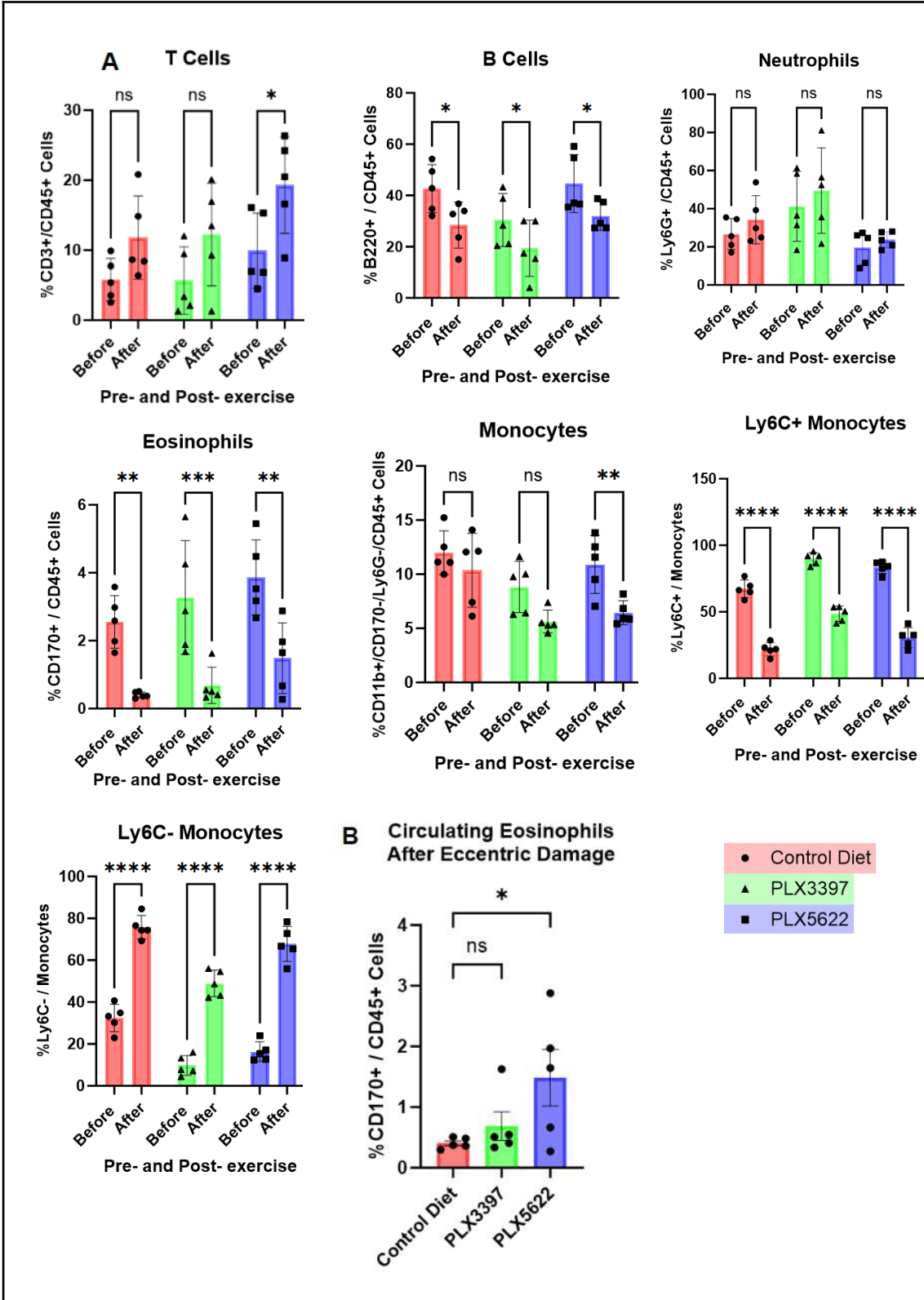


**Figure 5. (A)** The Effect of exercise induced eccentric damage on the immune cell population in the blood of *mdx* mice. **(B)**The Effect of exercise induced eccentric damage on eosinophils comparing treatment strategy. Blood samples were collected the same day pre- and post-exercise and analysis was done by flow cytometry. Two-way Anova with post-hoc Tukey's multiple comparison test \* $p < 0.05$ ; \*\* $p < 0.01$ ; \*\*\* $p < 0.001$ ; \*\*\*\* $p < 0.0001$ .

***Twenty-week CSF1R-inhibitor treatment changes proportions of skeletal muscle tissue-resident macrophages and fibro-adipogenic progenitors after contraction-induced damage.***

Next, using flow cytometry at the 28 week end-point after exercise, we evaluated the population dynamics of various resident cell types in the spleen and the skeletal muscle, specifically the Tibialis Anterior, Quadriceps and Gastrocnemius. There was no significant difference in number of tissue-infiltrating macrophages for either the inhibitors compared to the control (Figure 6A). Interestingly, we observed a change in proportions of tissue-infiltrated macrophages in the mice treated with the PLX3397 reporting an increase of Ly6C<sup>-</sup> macrophages in the skeletal muscle (Figure 6C). We also report a significant change in proportion of Ly6C<sup>-</sup> MHCII<sup>-</sup> and Ly6C<sup>-</sup> MHC-II<sup>+</sup> tissue-infiltrating macrophages in the mice treated with both inhibitors (Figure 6D). We further investigated the dynamics of SRRMs in skeletal muscles. Only PLX3397 reduced the population of SRRMs to a statistically significant extent as compared to the control group, while PLX5622-treated muscle had a considerable level of Tim4<sup>+</sup> cells remaining in the tissue (Figure 6B). Muscle stem cells (MuSCs), fibro-adipogenic progenitors (FAPs), endothelial and mural cells were elevated in mice treated with both CSF1R inhibitors (Figure 7). We observe a significant increase in number for endothelial and MuSCs only in PLX3397, while mural cells are significantly higher in both conditions. Only PLX5622 treatment group FAPs were significantly increased (Figure 7). Moreover, we observed that the FAP subpopulation dynamics were altered in the skeletal muscles of mice treated with both PLX3397 and PLX5622, whereby the proportion of CD26<sup>+</sup> FAPs was elevated (Figure 7).

At the 28-week mark, in addition to collecting the skeletal muscle, we analyzed the spleen using flow cytometry in order to understand more about the dynamics of the immune cell populations and compare them with the circulating immune cells (Figure 8). Interestingly we do not observe any significant differences in the number of immune cells in the spleen of animals treated with both compounds when compared to the control. Eosinophils are the only cell type that augments in the PLX5622 mice. The fraction of monocytes varies dramatically in the mice treated with PLX3397, despite the fact that the total number of monocytes in the spleen does not change. Indeed, we report a substantial decline in the ratio of Ly6C<sup>-</sup> to Ly6C<sup>+</sup> monocytes (Figure 8).

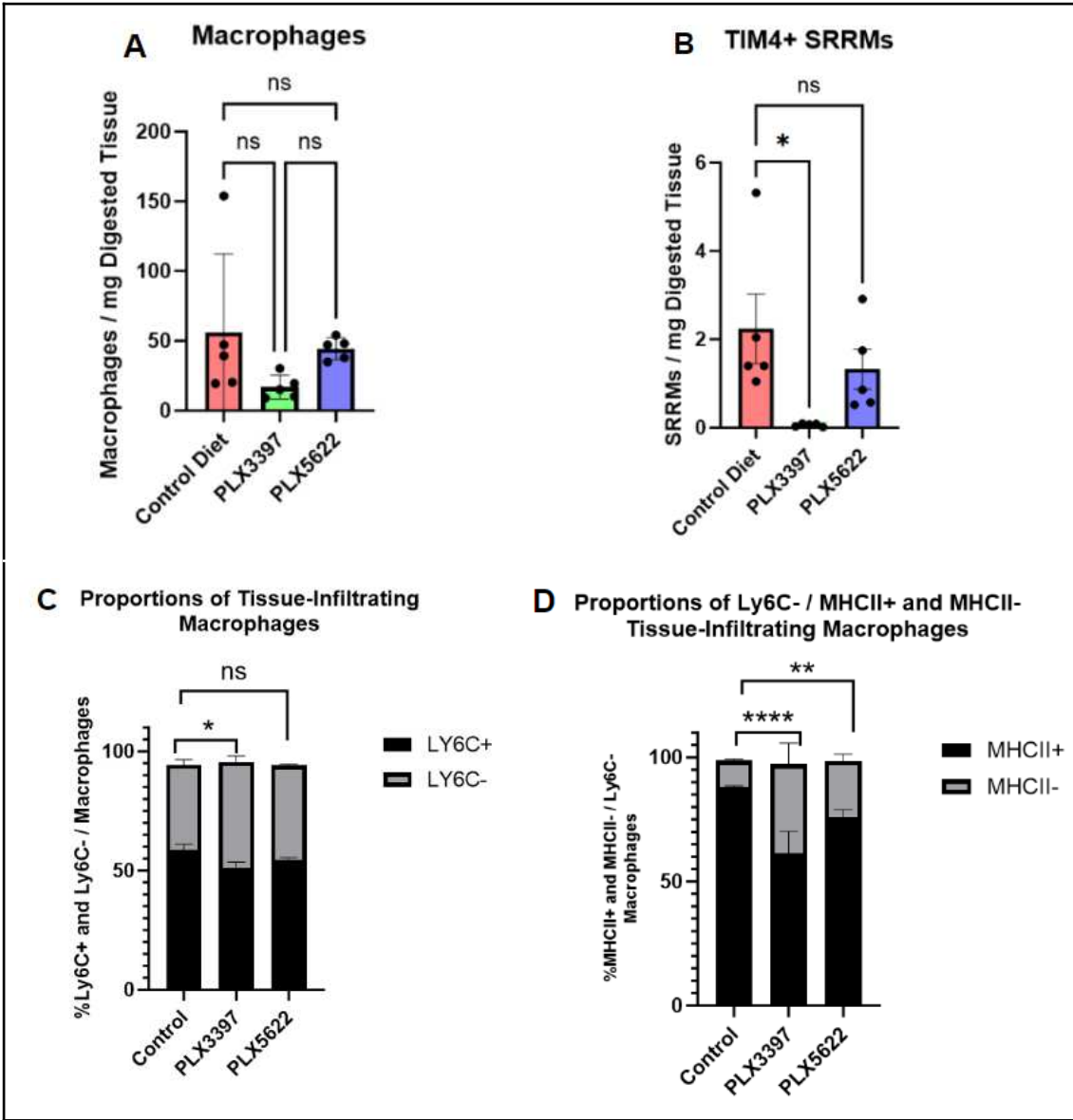


**Figure 6.** Macrophage populations in the skeletal muscle assessed by flow cytometry. Two-tailed Welch's t-test for Tim4+ comparisons. One-way Anova with post-hoc Tukey's 's multiple comparison test for FAP population analyses. \*p<0.05; \*\*p<0.01; \*\*\*\*p<0.0001;. Error bars represent the error of the mean.

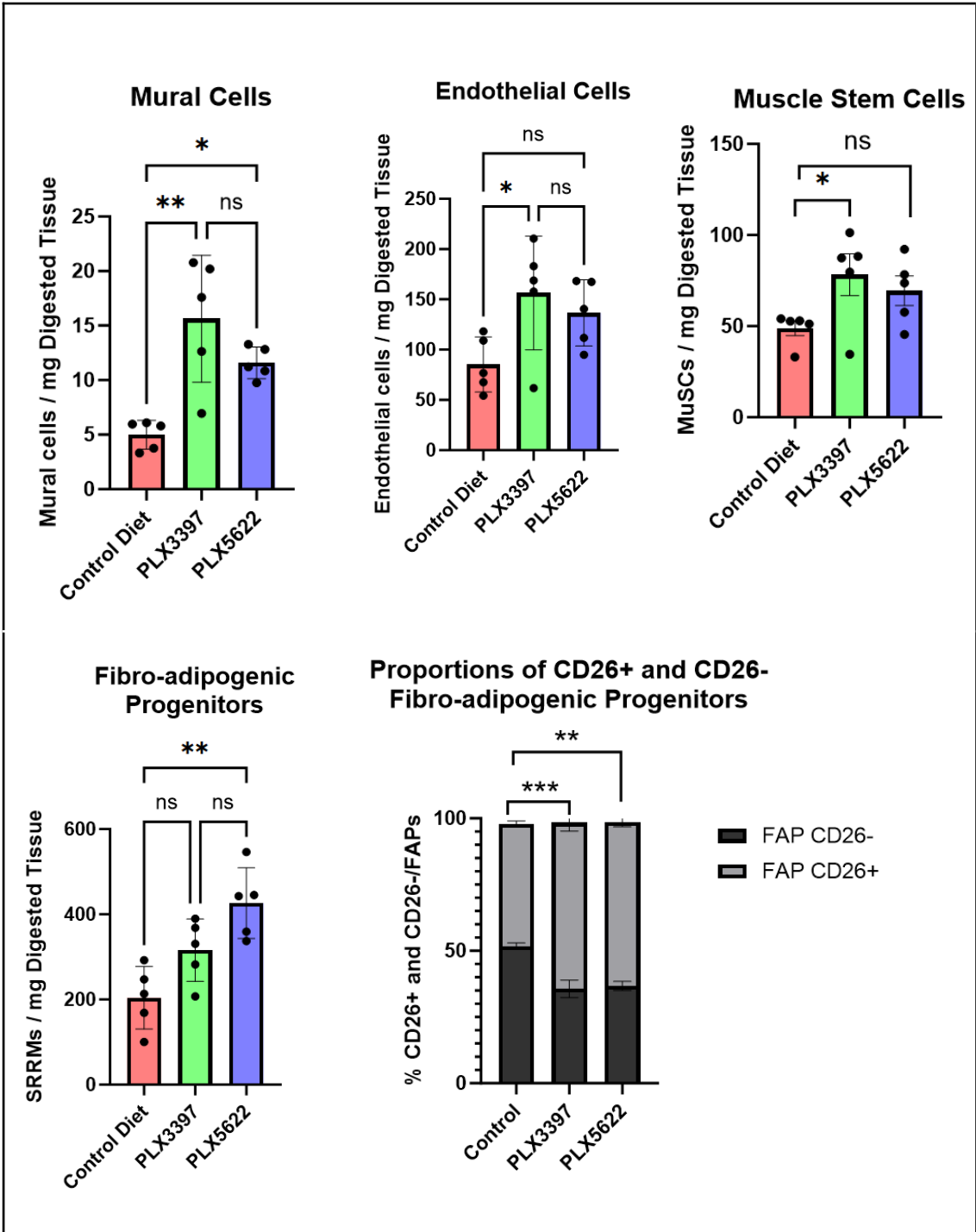


**Figure 7.** Resident cell types in the skeletal muscle assessed by flow cytometry. One-way Anova with post-hoc Tukey's 's multiple comparison test for FAP population analyses. \* $p < 0.05$ ; \*\* $p < 0.01$ ; \*\*\* $p < 0.001$ ;

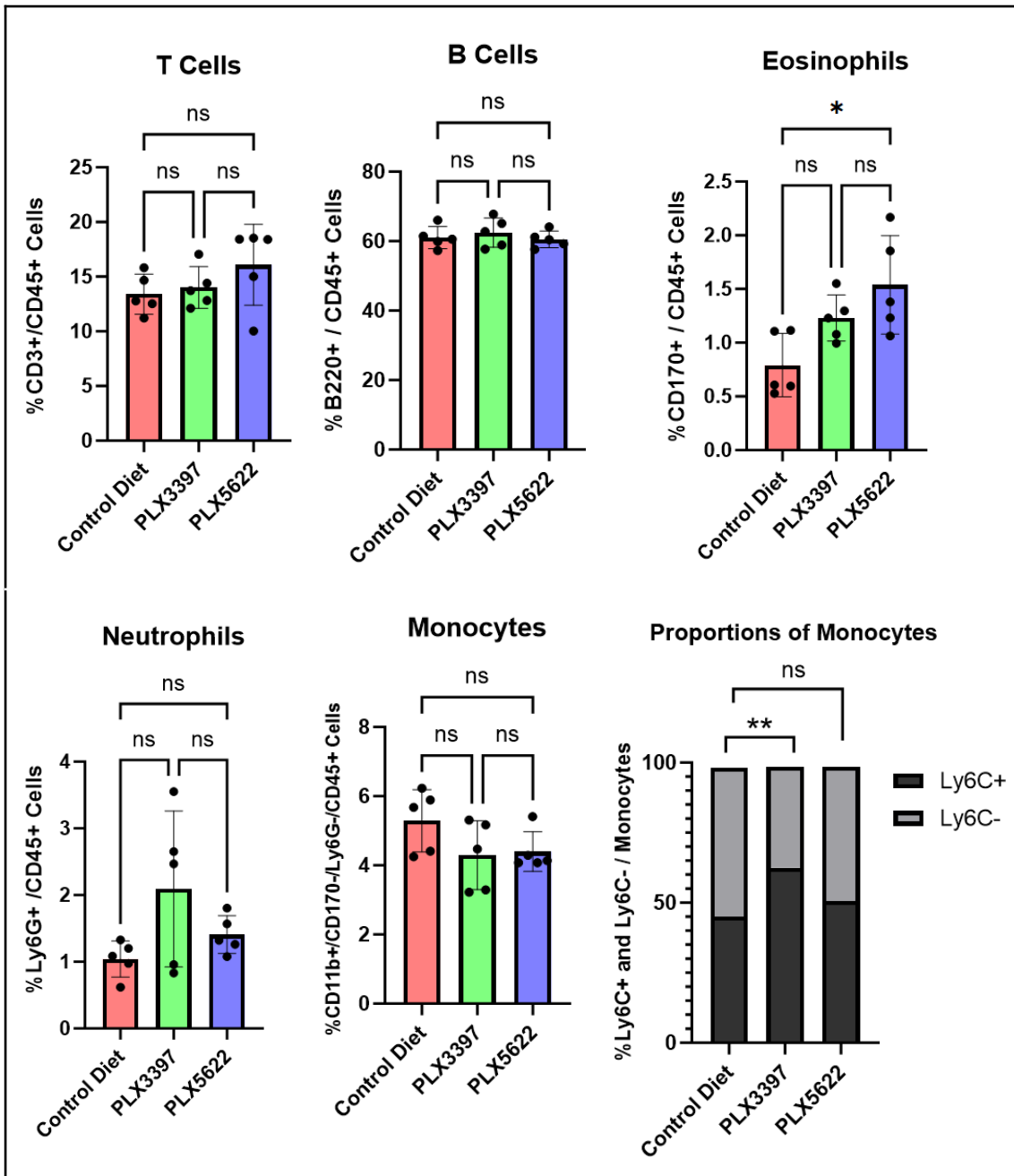
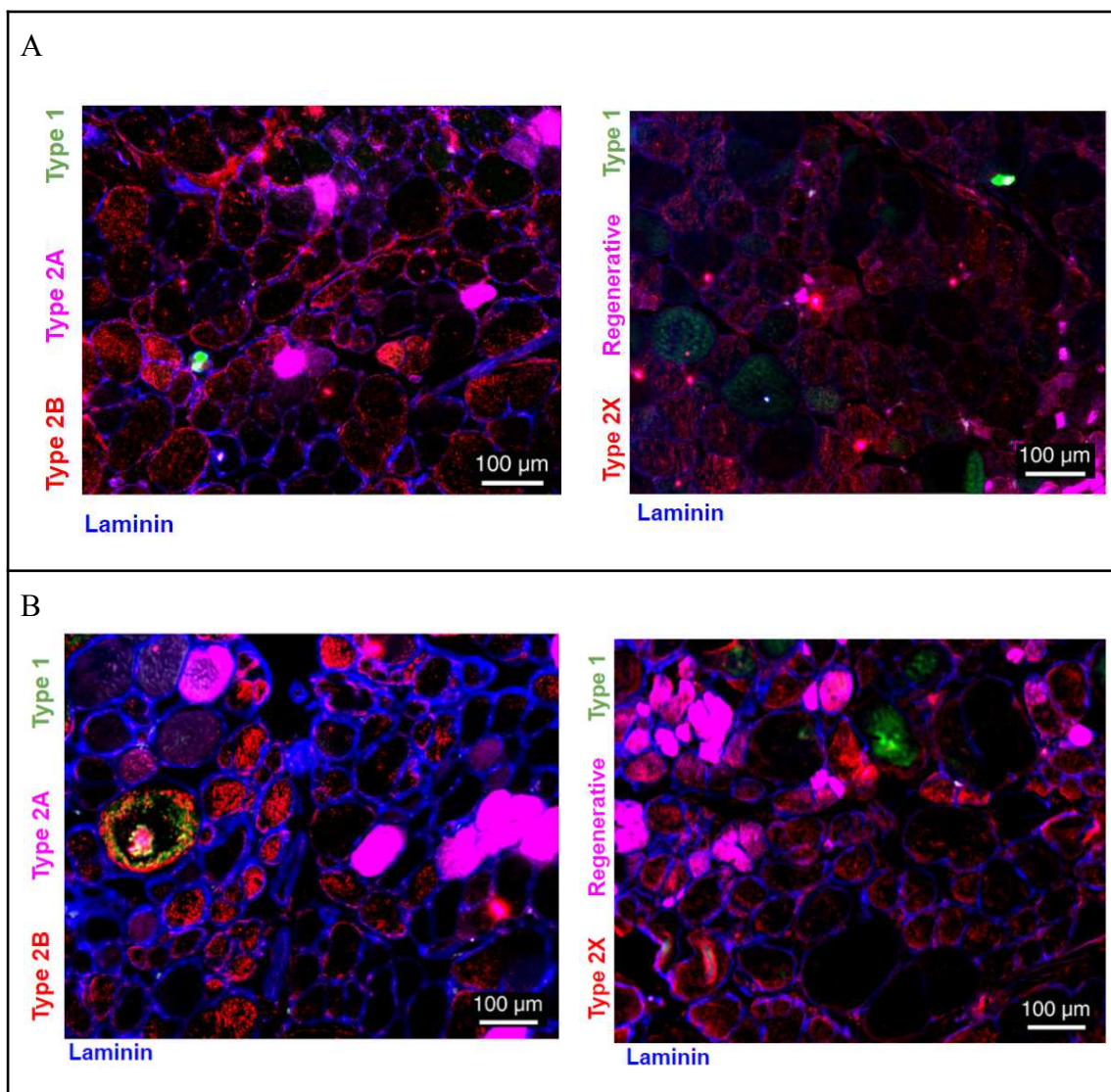


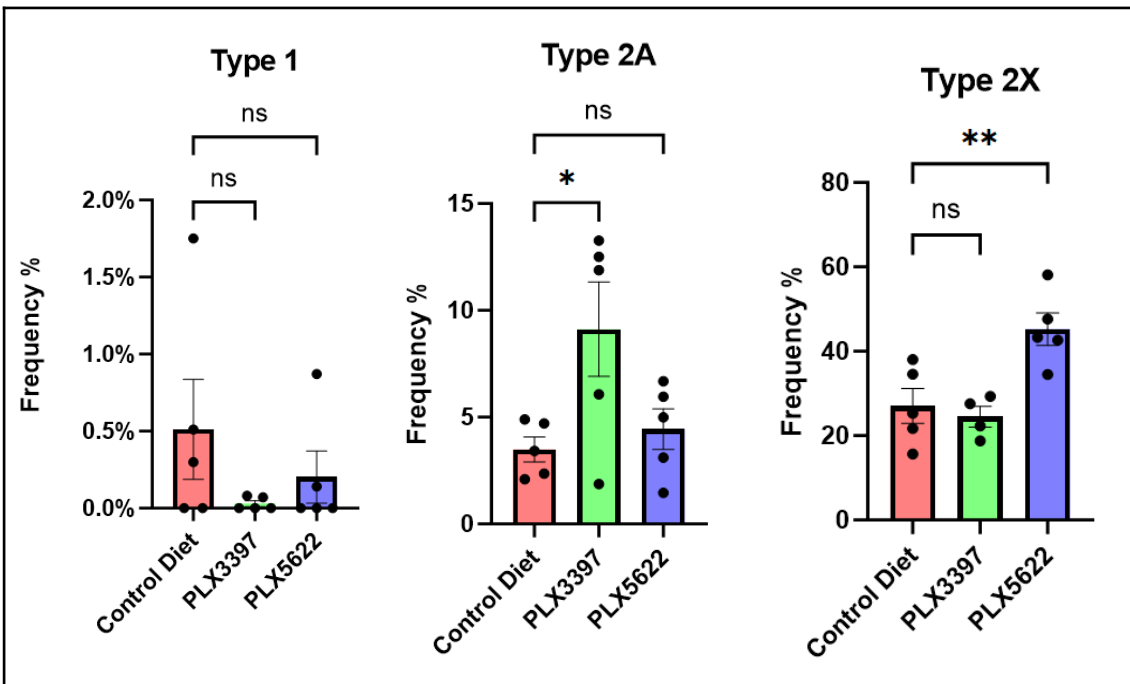
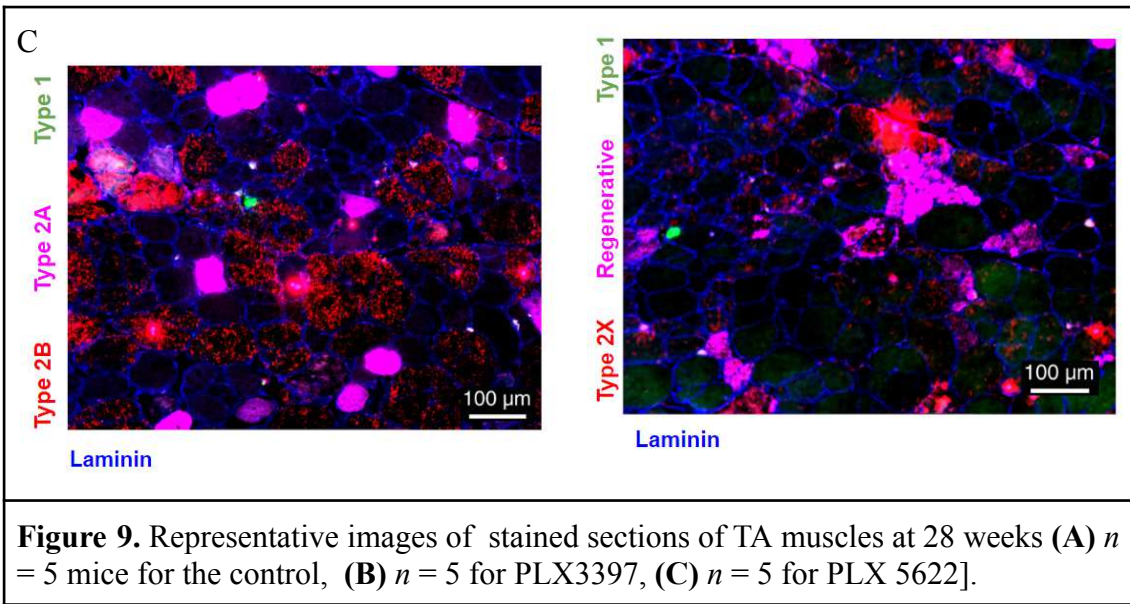
**Figure 8.** Spleen resident immune cell population dynamics at end-point, assessed by flow cytometry. One-way ANOVA with post-hoc Tukey's multiple comparison test. \* $p < 0.05$ ; \*\* $p < 0.01$ . Error bars represent the standard error of the mean.

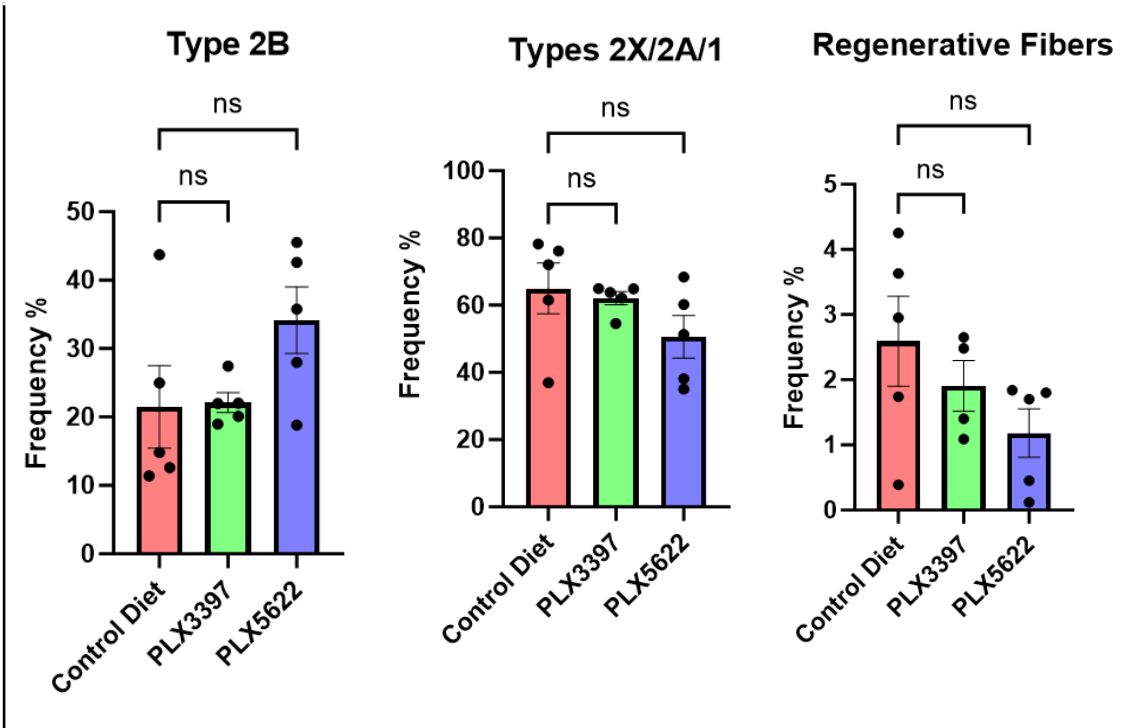
### *CSF1R inhibitors alter the metabolism of myofibers in mdx mice*

Previous research by our team has shown that long-term CSF1R inhibition leads to metabolic reprogramming of skeletal muscle (Theret et al., 2022). To further investigate the fiber-type composition of treated and untreated dystrophic muscle, we stained TA sections with antibodies against specific myosin heavy chain (MYH) proteins (Figure 9). There are very few type I (MYH7) fibers in the TA muscle. We observed a significant increase in the percentage of type IIA (MYH2) fibers with PLX3397

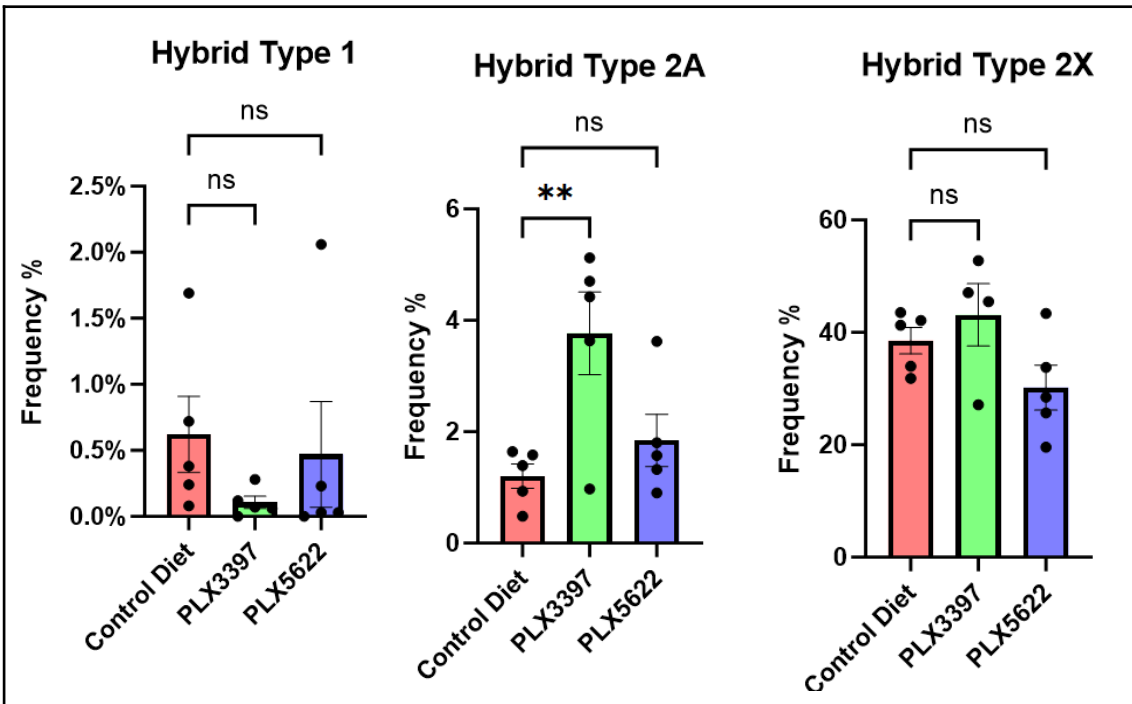
treatment. The percentage of type IIB (MYH4) and IIX (MYH1) fibers remained unchanged (Figure 10). Unstained fibers (non-IIB/IIA/I fibers) were mostly type IIX fibers with very few regenerating fibers expressing embryonic MYH3. Type IIX and type IIA fibers are more oxidative than type IIB fibers, indirectly suggesting that muscle treated with PLX3397, which has higher numbers of type IIA fibers, is more oxidative in its metabolic profile. Additionally, we wanted to assess potential differences in the quantity of hybrid fibers, as previous research has reported that 50% of muscle fibers in skeletal muscle of mammals are in fact hybrid (Heezen et al., 2023). Here, we reported a more pronounced significant change in the PLX3397 treated animals in comparison to the animals treated with PLX5622, when accounting for multiple MYH expression within the type 2A hybrid fibers, suggesting that after 20 weeks of treatment, metabolic reprogramming had occurred (Figure 11). We did not observe a significant change in the animals treated with PLX5622 compared to control chow group animals.







**Figure 10.** Effect of CSF1R inhibition on the type of muscle fibers in dystrophic TA. Quantification of the frequency of different fiber types is done on the total TA section. One-way ANOVA with post-hoc Tukey's multiple comparison test. \* $p < 0.05$ ; \*\* $p < 0.01$ . Error bars represent the standard error of the mean.



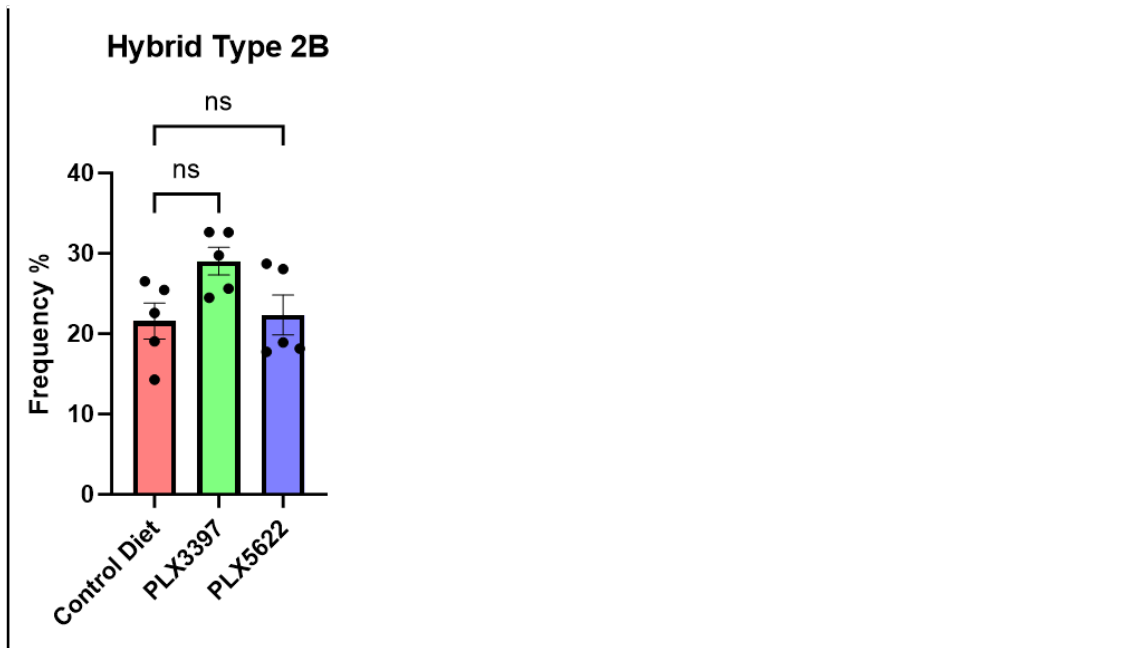


**Figure 11.** Effect of CSF1R inhibition on the hybrid types of muscle fibers in dystrophic TA. Hybrid fiber primary identity is defined by the marker with the highest expression. One-way ANOVA with post-hoc Tukey's multiple comparison test. \* $p < 0.05$ ; \*\* $p < 0.01$ . Error bars represent the standard error of the mean.

## DISCUSSION

Our study's primary goal was to evaluate the potential of CSF1R inhibitors for treating dystrophic mice. In order to do this, we designed a 20-week treatment plan that involved giving three groups of *mdx* mice either control chow or chow formulated with CSF1R inhibitors PLX3397 or PLX5622. We recorded the body weight of treated mice weekly throughout the course of the therapeutic timeline to examine the weight profile of dystrophic mice and compare the impact of CSF1R inhibition to the weight gain resulting from corticosteroid treatment, the current gold-standard for managing DMD patient pathology. Glucocorticoids are known to cause adverse effects, including osteoporosis, obesity, low stature, delayed puberty, and adrenal insufficiency (Duan et al., 2021). As such, our second objective was to compare the side effects of glucocorticoids, as the standard medication for DMD, with long-term CSF1R inhibition. We used an Analysis of Covariance to examine the effect of time and compared the effect of the two diets containing our therapeutic candidate compounds to the mice on the control diet group. The results demonstrated a substantial increase in weight with both tested inhibitors over time. Numerous animal studies have demonstrated that steroid-treated *mdx* mice lose weight in comparison to non-treated control animals, in contrast to steroid treatment in patients, which seeks to preserve muscle mass (Sali e al., 2012). Given the concurrent rise in muscle mass, we found an increase in mouse body weight with both CSF1R drugs in this preliminary dataset, which could be a favorable outcome.

To assess overall strength and endurance, we conducted muscle functional assays through assaying grip strength and treadmill running. The grip strength test is used in animal models of musculoskeletal degeneration to evaluate motor function and impairment. We evaluated grip strength on both the forelimbs alone and in combination with the hindlimbs, as enhancement in the performance in CSF1R inhibitor-treated mice was expected. The horizontal treadmill is a way to assess general motor skills and endurance in animal models of musculoskeletal degeneration. However, exercise on the treadmill in decline leads to a higher degree of contraction-induced damage on limb muscles, particularly on the TA. Contraction-induced damage occurs when muscles are stretched while contracting, forcing the muscle-tendon system to lengthen. Mechanical damage causes the injury, which is then followed by an inflammatory reaction. This procedure helps us understand the response of intermediate to acute inflammation in the setting of DMD as eccentric damage exacerbates the phenotype of muscle degeneration in the *mdx* mouse model. Having reported a significant positive weight gain in both treatment groups, accompanied by an increase in muscle mass in the TA, we were expecting the mice treated with the inhibitors to perform better in both the muscle strength assay as well as the endurance and resistance to eccentric stress. However, we did not observe an improvement in performance for the mice treated with the CSF1R inhibitors in either the fore-limb only, or the fore- and hindlimb combined grip strength tests. We reported a trend on exercise performance on the horizontal treadmill protocol, suggesting that the mice treated with the inhibitors had greater endurance. We observed a significant improvement in declined treadmill exercise only for the mice treated with the PLX5622 inhibitor, indicating this compound might improve resistance to eccentric stress.

We performed flow cytometry to allow deep immunophenotyping of the predominant cell populations in the spleen and in circulation. Based on our previous publication (Babaeijandaghi et al., 2022), we hypothesized that the animals treated with the CSF1R inhibitors would report a higher percentage of Ly6C<sup>+</sup> monocytes. This is due to the fact that Ly6C<sup>+</sup> monocytes are normally drawn to the damaged area, where they differentiate into tissue-resident macrophages (Theret et al., 2022). Nonetheless, we anticipate that this differentiation axis will be hampered by the suppression of the CSF1/CSF1R axis, increasing the amount of Ly6C<sup>+</sup> monocytes in the bloodstream. Interestingly we observed a significant drop in circulating monocytes as a result of exercise, however no significant difference was observed in the condition of resting state. Additionally, we observed that inhibition of CSF1R did not cause a significant change in monocyte presence. However, a dramatic change in the level of Ly6C expression in circulating monocytes was observed at resting state. Though only PLX3397 maintained a significantly higher proportion of Ly6C<sup>+</sup> monocytes after eccentric stress induced damage to skeletal muscle. Instead, animals treated with PLX5622 seemed to restore the balance between Ly6C<sup>+</sup> versus Ly6C<sup>-</sup> circulating monocytes after exercise on the treadmill in decline, resembling the profile observed in the control group. We hypothesize that inhibition of CSF1R is impairing the conversion

of Ly6C<sup>+</sup> to Ly6C<sup>-</sup> patrolling monocytes, as previous studies have shown higher expression of CSF1R on Ly6C<sup>+</sup> monocytes (Robinson et al., 2021). Additionally, we observe a decrease in Ly6C<sup>+</sup> tissue infiltrating macrophages, as CSF1R is responsible for the recruitment and differentiation of Ly6C<sup>+</sup> monocytes to Ly6C<sup>+</sup> macrophages in dystrophic tissue (Robinson et al., 2021). Therefore, our findings suggest that Ly6C<sup>+</sup> monocytes are retained in circulation in *mdx* mice treated with PLX3397, both at steady state and following contraction-induced damage, whereas *mdx* mice treated with PLX5622 appeared to have a different recruitment pathway that may be triggered in response to intermediate or acute damage.

Our observations reveal that the effect of exercise on immune cell dynamics in dystrophic mice is transient, as spleen-resident immune cell populations generally remain unchanged. With the exception of monocytes, our research demonstrates that exercise leads to a decrease in circulatory eosinophils in dystrophic animals, regardless of whether they are undergoing treatment or are in a control condition. Given that dystrophic muscle is more prone to muscle damage, the latter population would be reduced, presumably as a result of skeletal muscle infiltration, where they produce cytokines such as IL-4, IL-13 and TGF-beta, which in turn have the ability to control inflammation.

### ***The effect of CSF1R inhibition on self-renewing tissue resident macrophages***

Our research group has previously shown that treating *mdx* mice with CSF1R inhibitor PLX73086 completely depleted the TIM4<sup>+</sup> self-renewing tissue resident macrophages (Babaeijandaghi et al., 2022). Therefore, we hypothesized that both our compounds could show similar results. Interestingly, PLX3397-treated mice lacked the TIM4<sup>+</sup> SRRMs population in skeletal muscle at the study end-point, while TIM4<sup>+</sup> macrophages were still present in PLX5622-treated muscle, at a similar level to the control group of animals. We can speculate that the SRRMs of the mice treated with PLX5622 may develop a survival strategy that is independent of CSF1, allowing them to outcompete the inhibitor's harmful effects brought about by the highly specific chemical structure. To test this hypothesis in the future, we can administer a short-term treatment (21 days) with PLX5622 and note the effect on TIM4<sup>+</sup> SRRMs. Should TIM4<sup>+</sup> SRRMs be depleted after 21 days, two conclusions would follow: 1) tissue-resident macrophages are vulnerable to CSF1Ri-mediated depletion in the short term; 2) tissue-resident macrophages in *mdx* mice must be transitioning to a CSF1-independent route for long-term survival. On the other hand, if the inhibitor does not deplete TIM4<sup>+</sup> SRRMs, these cells have inherent survival benefits over PLX5622. Furthermore, our results also suggest less side-effects from partial instead of complete elimination of SRRMs which is required for the homeostatic balance of other muscle cell populations like the CD26<sup>+</sup> proportion of fibro adipogenic progenitors. We observed a significant increase in the proportion of CD26<sup>+</sup> to CD26<sup>-</sup> FAPs with both CSF1R inhibitors. The CD26<sup>+</sup> subpopulation has recently been reported as a higher

order progenitor within the general population of FAPs (Huang et al., 2021). FAP numbers need to be cautiously monitored in dystrophic muscle as their uncontrolled expansion leads to tissue fibrosis, as previously shown by Lemos et al., 2013. Unfortunately, with this experimental setup it is hard to determine whether the observed effects primarily result from the prolonged treatment with CSF1R inhibitors or if they are simply a temporary response triggered by the inflammatory reaction induced by eccentric damage.

### ***Polarization of tissue-infiltrating macrophages via the CSF1/CSF1R and CSF2/CSF2R Axis***

Upregulation of the CSF2/CSF2R (also called GM-CSFR) axis could be another possible explanation for the increase in Ly6C<sup>+</sup> monocytes and macrophages (Figure 12A). The structure of the CSF2 receptor differs significantly from that of the CSF1R; it is a heterodimeric receptor made up of the  $\beta$  common subunit (CSF2RB) and the  $\alpha$  subunit (CSF2RA), therefore it is not targeted by neither of the PLX compounds. The activation of signaling pathways by CSF2R upon CSF2 ligand binding is crucial for the proliferation, development, and survival of macrophages and granulocytes. The CSF2/CSF2R pathway is responsible for the polarization of Ly6C<sup>+</sup> monocytes and macrophages, in contrast to CSF1/CSF1R signaling, which induces Ly6C<sup>-</sup> polarization (Cai et al., 2021). Both monocytes and macrophages feature constitutive expressions of CSF1R and CSF2R on their cell membranes (Hume et al., 2011).

Previous research has shown a compensatory mechanism that increases CSF2R expression triggered by inhibition of the CSF1/CSF1R axis in tumor single-cell suspensions (Van Overmeire et al., 2016), which would explain the observed increase in Ly6C<sup>+</sup> monocytes and macrophages. As such, we would expect tissue-infiltrating macrophages to undergo repolarization via the CSF2/CSF2R axis, resulting in the acquisition of a Ly6C<sup>-</sup> phenotype (Figure 12). Major Histocompatibility Complex-II (MHC-II) expression is upregulated in macrophages that express CSF2 (Van Overmeire et al., 2016). Macrophages that express MHC-II molecules play critical roles in the immune system. MHC-II molecules are responsible for presenting antigens to CD4<sup>+</sup> T cells, which are a type of T lymphocyte involved in orchestrating immune responses (Lendeckel et al. 2022). By utilizing the flow data obtained from the harvested skeletal muscle of all the experimental groups, we compared the Ly6C<sup>-</sup> macrophages that expressed MHC-II and those that did not. Interestingly, there was a significant drop in LY6C<sup>-</sup> MHC-II<sup>+</sup> tissue infiltrating macrophages in the animals treated with both the CSF1R inhibitors, with a more significant difference observed in the animals treated with PLX3397. Unfortunately, we did not examine for variations in the numbers of CD4<sup>+</sup> and CD8<sup>+</sup> T-cells that circulate in the blood or enter tissues. Therefore, we are unable to determine whether the variation in Ly6C<sup>-</sup> MHC-II<sup>+</sup> that we see between the animals given the control diet and those given the CSF1R inhibitor has an impact on the tissue infiltrating macrophage's ability to recruit T cells.

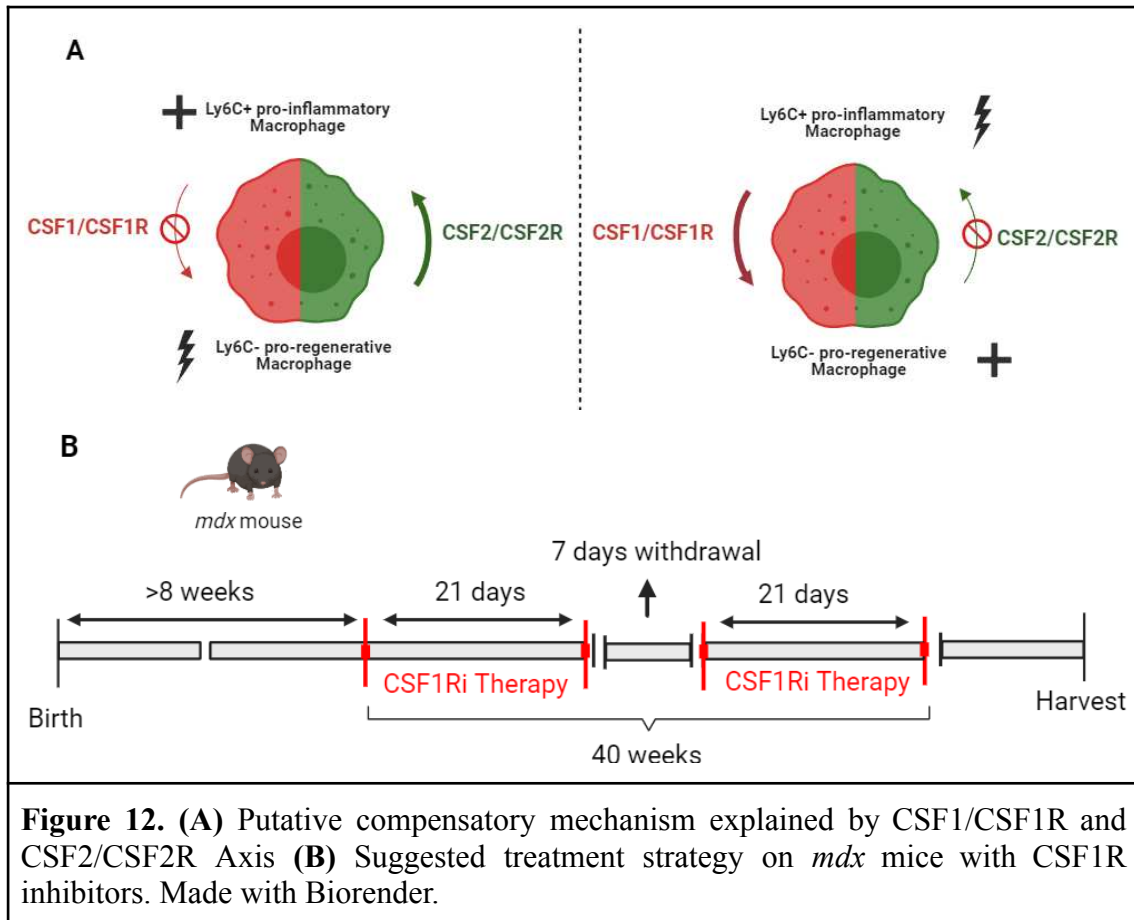


**Figure 12. (A)** Putative compensatory mechanism explained by CSF1/CSF1R and CSF2/CSF2R Axis **(B)** Suggested treatment strategy on *mdx* mice with CSF1R inhibitors. Made with Biorender.

### *Metabolic reprogramming of muscle fibers in PLX3397-treated mdx mice*

Skeletal muscles display a wide range of physiological characteristics influenced by factors like exercise, disease, and development. The adaptability of skeletal muscle is partly attributed to myosin heavy chain (MHC) proteins. Among the eleven MHC isoforms, only six are consistently found in limb skeletal muscles, significantly impacting muscle properties like shortening velocity and power production (Brummer et al., 2013). Various fiber types, such as Type I, IIA, IIX, and IIB, result from different MHC isoforms. In addition to the single fiber types that express only one MHC isoform, a large number of fibers are hybrids, as they co-express two or more distinct MHC or other myofibrillar protein isoforms (Heezen et al., 2023). Notably, tibialis anterior (TA) muscle shows a prevalence of hybrid fibers during postnatal development, gradually declining in adulthood. The role of hybrid fibers in muscle development is intricate and undergoes dynamic changes over time. These patterns reveal that the role of hybrid fibers as intermediates in muscle development is complex (Brummer et al., 2013). We expect a significant metabolic shift of the dystrophic muscle to be evident through the hybrid fibers as they act as intermediaries in muscle development, exercise adaptation, and aging, contributing to a diverse range of muscle phenotypes. As hypothesized, we observed a significantly higher number of type 2A hybrid fiber, demonstrating that active metabolic reprogramming is occurring with the 20 weeks treatment with PLX3397. Type 2A fast oxidative-glycolytic fibers exhibit a combination of

characteristics from both fast-twitch and oxidative fibers. Compared to other types of muscle fibers, these fibers are known for being more resistant to damage. Compared to type 2B fast-twitch fibers, they have a higher oxidative capacity due to their larger number of mitochondria, which lowers the intracellular accumulation of reactive oxygen species. As such, higher number of type 2A fibers indicates a less oxidative environment in the dystrophic muscle, post-exercise and eccentric damage. This is a positive outcome of the treatment as we previously explained that a highly oxidative environment and inability to neutralize reactive oxygen species all contribute to fast degeneration of the myofibers.

## CONCLUSION

Research conducted by our group has indicated that self-renewing tissue-resident macrophages serve as the initial responders to acute inflammation, possibly due to their role in initiating phagocytosis. Instead, tissue-infiltrating Ly6C<sup>+</sup> macrophages, identified as pro-inflammatory macrophages, are activated in acute injury models and remain elevated in the tissue for approximately 2 weeks before reverting to baseline levels. In cases of chronic inflammation, Ly6C<sup>+</sup> macrophages do not return to their baseline levels and, instead, contribute to the overactivation of the TGF-beta signaling cascade (Theret et al., 2022). Tissue-infiltrating Ly6C<sup>-</sup> macrophages exhibit a pro-regenerative phenotype, producing TGF-beta that facilitates the differentiation of fibro-adipogenic progenitors (FAPs) into fibroblasts. In the context of a healthy muscle in a steady-state and following acute injury, Ly6C<sup>-</sup> macrophages return to baseline levels after 14 days (Theret et al., 2022). However, in chronic inflammation settings, Ly6C<sup>-</sup> macrophages accumulate, contributing to the buildup of non-functional fibrotic scar tissue, necrotic areas, and the presence of adipocytes. Moreover, in *mdx* dystrophic muscle, the heightened numbers of both Ly6C<sup>+</sup> and Ly6C<sup>-</sup> macrophages establish a persistent cycle of cytokine release and inflammatory responses (Theret et al., 2022; Li et al., 2022). Our findings suggest that PLX5622 may be more advantageous as a short-term intervention, more adapted to promote muscle regeneration in models of acute injury, than as a long-term therapy for models of chronic inflammation, while PLX3397 shows greater potential as a long-term treatment strategy. We suggest a potential therapeutic approach involving the repeated administration of the CSF1R inhibitor, followed by a short-term withdrawal period (Figure 12B).

This is because the CSF1/CSF1R axis triggers the accumulation of pro-inflammatory Ly6C<sup>+</sup> macrophages in the tissue, facilitating the initiation of a short-term inflammatory response that closely resembles what is observed in the context of the acute injury model. The transient buildup of Ly6C<sup>+</sup> infiltrating macrophages will result in the phagocytosis and apoptosis of necrotic tissue, leading to a decrease in intracellular oxidative stress. Upon withdrawal of treatment with CSF1R inhibitor, we anticipate a shift in the pro-inflammatory Ly6C<sup>+</sup> macrophages toward a pro-regenerative Ly6C<sup>-</sup>

phenotype. The transient accumulation of Ly6C<sup>-</sup> macrophages is expected to promote tissue regeneration via the TGF-beta pathway, while limiting fibrosis and adipogenesis. This potential outcome might be facilitated by the compensatory mechanism of the CSF2/CSF2R axis, through the polarization of pro-regenerative Ly6C<sup>-</sup> macrophages into pro-inflammatory Ly6C<sup>+</sup> macrophages, as documented in previous literature (Li et al., 2022; Klemm et al., 2021). To test this hypothesis we would add an additional group of *mdx* mice treated with CSF2R inhibitors and compare the expression profile of circulating monocytes, tissue-infiltrating macrophages and self-renewing tissue resident macrophages between the mice treated with the CSF1R inhibitor.

## **MATERIALS AND METHODS**

### Mice

C57BL/6J, C57BL/10ScSn-Dmdmdx/J (Dmdmdx) mice were purchased from The Jackson Laboratory.

### CSF1R Inhibitors

We used two different CSF1R inhibitors in our study: PLX5622 and PLX3397. PLX5622 has the name of hemifumarate and the code of HY-114153A: it is used with a concentration of 1200 mg/kg in diet. PLX3397 has the name of Pexidartinib and the code of AIN-76A and it is used with a concentration of 290 mg/kg. Both diets and control chow are kept at room temperature.

### Treadmill exercise protocol

The exercise protocol for assessing endurance in *mdx* mice treated with either PLX3397, PLX5622, or control chow involves a weekly regimen during weeks 17, 18, 19, and 20 of the treatment plan to accentuate the pathology. This allows for the longitudinal evaluation of their performance over time. The animal treadmill (Exer 3/6, Columbus Instruments) is set to a decline of  $-16^{\circ}$  with a low intensity electric shocker of 2 Hz. All animals complete a one-week acclimatization period during week 17. For the acclimatization the protocol follows 2 minutes with the 2 Hz shocker on (lowest intensity). The treadmill is stationary (0 m/min), and this period is to allow the mice to explore the environment. Two min at 2.5 m/min, 2 min at 5 m/min and finally, 2 min at 7.5 m/min. Following a single session, we introduced a blunt object as a conditioned stimulus to gently poke the mouse when it approaches the shocker grid. The experimental protocol begins with a warm up at 7.5 m/min for 5 minutes, followed by a 10 m/min for 15 minutes and a 12.5 m/min pace for 30 minutes. We measure speed, distance traveled and time. We then derived work and power using  $Work (J) = body\ mass (kg) \times gravity (9.81\ m/sec^2) \times vertical\ speed (m/sec \times angle) \times time (sec)$  and  $Power (W) = work (J)/time (sec)$  as indicated in Castro et al., 2017. The experiment concludes when the mouse is no longer able to run forward and opts to sit on the edge of the shocker, even with gentle nudging for motivation. Continuous supervision is

necessary, and the shocker is promptly turned off upon reaching any of these endpoints. Thirty minutes post-exercise, blood is drawn from the saphenous vein and analyzed using flow cytometry. The objective of this experiment is to assess mouse endurance, fatigue levels, and in vivo muscle injury in response to the specified treatment.

### Grip test

The purpose of this test is to evaluate motor performance and limb strength and insurance in *mdx* mice. The animal's paws are placed on a wire grid, which the animal will naturally hold on to while its tail is gently pulled backwards. The maximum strength of the grip prior to grip release is recorded. The test was performed in one session per week with each session consisting of three trials, in weeks 17, 18, 19 and 20. The animal's average performance for each session is presented as the average of the three trials and normalized to the mice body weight.

### Muscle digestion and flow cytometric analysis

Mice were anesthetized with Avertin (Sigma-Aldrich, T4840-2) administered through an intraperitoneal injection of 750ul, followed by perfusion with room-temperature with 10 ml of 1X PBS containing 2 mM EDTA. The weight of the mouse was recorded before perfusion. We harvested the following skeletal muscles: Tibialis Anterior, Quadriceps and Gastrocnemius, after removing the fascia. Single weights per muscle were recorded before tissue digestion. Skeletal muscles were pulled as a single sample and cut into small pieces using scissors. Tissue enzymatic digestion was done with a mixture of collagenase D (1.5 U ml<sup>-1</sup>; Roche # 11088882001) and dispase II (2.4 U ml<sup>-1</sup>; Roche # 04942078001) and CaCl<sub>2</sub> (10 ul for 1 ml) for an hour at 37 °C on a rotating platform. Samples were vortexed every 15 minutes during incubation time. After one hour of incubation, the digestion was stopped with 1ml of cold FACS buffer and the digested tissues were filtered first through a 40 and then through a 70-µm cell strainer (Falcon, # 352340). Washes were done with 1X PBS and the pellet was collected by centrifugation at 545g for 10 minutes. Cells were then blocked in FACS blocking buffer made with 1X PBS containing 2 mM EDTA and 2% FBS (FACS buffer) and an anti-Fcγ receptor antibody at 4 °C for 30 minutes and then stained with various antibodies at 4 °C for 30 minutes. Stained cells were washed using a FACS buffer for a total of 3 washes and analyzed using CytoFlex LX (Beckman Coulter). Skeletal muscle panel antibodies are CD45-488 (1:500), CD31-FITC (1:500), VCAM-Biotin (1:2,000), VCAM-PE 1/1k (1:500), Itga7-A647 (1:3,000), Sca1-PECy7 (1:4,000), Anti-TIM4 PE/Cy7 (1:200), Anti-LYVE1 eFluor 450 (1:500), Anti-CD11B Brilliant Violet (1:500), Anti-CD170 (SIGLEC F) PerCP-eFluor (1:500), Anti-CD11C 488 (1:500), Anti-LY6G PerCPCy (1:500), Anti-F4/80 PE (1:200), Anti-F4/80 APC (1:200), Anti-LY6C Alexa Fluor®647 (1:500), Anti-LY6C PE/Cy7 (1:800), Anti-Fc Receptor 24G2 (1:200).

### Immune cell analysis from blood and spleen

Tissue enzymatic digestion was done with a mixture of collagenase D (1.5 U ml<sup>-1</sup>; Roche # 11088882001) and dispase II (2.4 U ml<sup>-1</sup>; Roche # 04942078001). Mixture should be 1ml per tissue and the total weight of the tissue should not be more than 300mg. For tissues, we used 2 ml flat bottom Eppendorf tubes with 1 ml of 1X PBS. Instead, for blood, we used regular 1.5ml Eppendorf with 1 ml of 1X PBS EDTA, to avoid coagulation. Mice were anesthetized with Avertin (Sigma-Aldrich, T4840-2) administered through an intraperitoneal injection of 750ul. The weight of the mouse was recorded before perfusion with 10 ml of 1X PBS containing 2 mM EDTA. After the mouse was unresponsive, we opened the chest cavity and harvested 100 ul of blood directly from the heart with a 27g needle on top of a 1ml syringe and the needed tissues. The tissue was filtered first through a 40 and then through a 70- $\mu$ m cell strainer (Falcon, # 352340). Cells were centrifuged at 400g for 7 minutes at 4°C and supernatant was discarded, before resuspending the pellet in 200ul of FACS buffer per staining.

For the blood preparation, blood was centrifuged at 500g for 5 minutes at 4 °C. We then removed the supernatant and added 1 ml of ACK lysis buffer to lyse red blood cells. We vortexed and incubated for another 10 minutes at room temperature, before repeating the centrifugation step at 500g for 5 minutes at 4 °C. After removing the supernatant, we performed a second round of lysis. The pellet was then resuspended to have a final volume of 200ul per staining. The samples are distributed in 96 well plates.

The following steps were the same for both blood and tissues. We add 100ul of FACS blocking buffer per well and we incubate for 30 minutes at 4 °C. We then added 100ul of the antibody mix in addition to the FACS blocking buffer and we repeated incubation for 30 minutes at 4 °C. Stained cells were washed using a FACS buffer for a total of 3 washes and analyzed using CytoFlex LX (Beckman Coulter). Antibody mixes were all with dilutions of 1X for the Eosinophils and Macrophages: Ly6G- PerCEPc5.5 (1:400), NK1.1 PerCPC5.5 (1:200), CD3e PerCPC5.5 (1:400), CD45-PB (1:400), CD11b-BV605 (1:500), CD11c-FITC (1:400), CD34-FIT (1:200), Ly6C-PeCy7 (1:800), SiglecF-APC (1:400)

### Histology

For immunofluorescence microscopy, fresh samples were embedded in O.C.T. compound (Tissue-Tek®, Sakura, # 4583) and kept at -80 °C. All sections have a thickness of at 10  $\mu$ m and are done using a Leica Cryostat. Sections are rinsed in PBS for 10 to 30 seconds and permeabilized using 0.5% Triton X-100 for 10 minutes. Section were blocked in blocking buffer with PBS containing 0.3% Triton X-100, 2% BSA, 5% Glycine and MOM block in TBST (Sigma-Aldrich, #T8787) and 2% normal goat serum at room temperature for an hour. Samples were stained with different antibodies in the blocking buffer targeting different myosin heavy chains for 45 minutes at room temperature. After three washes with PBS containing 0.3% Triton and glycine,

samples were incubated with secondary antibodies for 45 minutes at room temperature before further washing. The sections are covered with Fluoromount G (Southern Biotech, # 0100-01) and a cover slip and imaged using Nikon Eclipse (NIS 344 Elements v5.11.03 software) or Zeiss LSM900 confocal (ZEN Blue v3.4.91.00000 software) 345 microscopes. The analysis was performed on ImageJ or the Nikon NIS-Element software. Antibodies from Developmental Studies Hybridoma Bank: Myosin Heavy Chain Type I BA-D5 5 ug/mL, Myosin Heavy Chain Type IIA SC-71 5 ug/mL, Myosin Heavy Chain Type IIX 6H1 7 ug/mL, Myosin Heavy Chain Type IIB BF-F3 5 ug/mL, Myosin Heavy Chain Embryonic F1.652 5 ug/mL and Anti-laminin Polyclonal (1:200) from AbCam. The list of secondary antibodies follows Goat anti-Mouse IgG (H+L) AlexaFluor 647 (1:1000), Goat Anti- Mouse IgG, Fc $\gamma$  subclass 1 specific Alexa488 (1:200), AffiniPure Goat Anti-Mouse IgG, Fc $\gamma$  subclass 2b specific DyLight™ 405 (1:200), AffiniPure Goat Anti-Mouse IgM,  $\mu$  chain specific Alexa Fluor594 (1:200).

#### Statistical Analysis

The data in the figures are presented as mean with the error bars showing the standard error of the mean (SEM). All statistical analysis and graphs were done using GraphPad Prism 9. We used parametric t tests and analysis of variance (ANOVA) for statistical comparison. Statistical comparison was performed using unpaired t test. To compare multiple groups, we used one-way ANOVA. If the test showed no significant difference between SDs, ordinary one-way ANOVA followed by a proper multiple comparison test was performed. For multiple comparisons, Tukey's tests were used comparing every mean with every other mean. The mice's weights were compared using ANCOVA analysis. ANCOVA is an analysis of variance that considers continuous values, in this instance time.

#### Fiber typing quantification

For each image, Regions Of Interest (ROI) were generated from a Laminin stained section. Laminin staining was run through a deep learning algorithm (Cellpose v2.0) using the Cyto2 model. Default settings were used, if not otherwise specified. Specific settings were: Flow Threshold = 0.4. Cell Probability Threshold = 0.0. Diameter = Cellpose auto estimation. For each set of ROIs and images, each fiber's type was calculated from a myosin heavy chain stain using Fiji v1.54. The procedure for image processing and fiber typing was the same for each channel and for each sample. Processing steps were undertaken to remove background and reduce random noise. Fiji image processing steps: Subtract background (rolling radius parameter = 50). Enhance contrast (% saturated parameter = 0.5). Gaussian blur (sigma parameter = 5). Despeckle. Set Threshold (threshold = Otsu for all channels except CHANNEL2 with MAXENTROPY). Each fiber was then calculated. Each fiber showing more than 50% coverage in the channel threshold was determined to be positive for that channel. Negative fibers were determined to be fibers showing less than 20% coverage across all

channels. These fibers were determined to be the fiber type that didn't undergo staining. Hybrid fibers showed between 20% and 50% coverage in at least one channel.

## BIBLIOGRAPHY

1. Duan D, Goemans N, Takeda S, Mercuri E, Aartsma-Rus A. Duchenne muscular dystrophy. *Nature Reviews Disease Primers*. 2021;7(1):1-19. doi:<https://doi.org/10.1038/s41572-021-00248-3>
2. Paleo BJ, McElhanon KE, Bulgart HR, et al. Reduced Sarcolemmal Membrane Repair Exacerbates Striated Muscle Pathology in a Mouse Model of Duchenne Muscular Dystrophy. *Cells*. 2022;11(9):1417-1417. doi:<https://doi.org/10.3390/cells11091417>
3. Dumont NA, Wang YX, von Maltzahn J, et al. Dystrophin expression in muscle stem cells regulates their polarity and asymmetric division. *Nature Medicine*. 2015;21(12):1455-1463. doi:<https://doi.org/10.1038/nm.3990>
4. Mosca N, Petrillo S, Bortolani S, et al. Redox Homeostasis in Muscular Dystrophies. *Cells*. 2021;10(6):1364-1364. doi:<https://doi.org/10.3390/cells10061364>
5. Almeida-Becerril T., Rodríguez-Cruz M, Villa-Morales J, Christian Ricardo Sánchez-Mendoza, Jose Emilio Galeazzi-Aguilar. Circulating Nrf2, Glutathione, and Malondialdehyde Correlate with Disease Severity in Duchenne Muscular Dystrophy. *Antioxidants*. 2023;12(4):871-871. doi:<https://doi.org/10.3390/antiox12040871>
6. Mareedu S, Million ED, Duan D, Babu GJ. Abnormal Calcium Handling in Duchenne Muscular Dystrophy: Mechanisms and Potential Therapies. *Frontiers in Physiology*. 2021;12:647010. doi:<https://doi.org/10.3389/fphys.2021.647010>
7. Theret M, Saclier M, Messina G, Rossi FMV. Macrophages in Skeletal Muscle Dystrophies, An Entangled Partner. *Journal of Neuromuscular Diseases*. 2022;9(1):1-23. doi:<https://doi.org/10.3233/jnd-210737>
8. Osińska I, Popko K, Demkow U. Perforin: an important player in immune response. *Central European Journal of Immunology*. 2014;1(1):109-115. doi:<https://doi.org/10.5114/ceji.2014.42135>
9. Lazarov T, Juarez-Carreño S, Cox N, Geissmann F. Physiology and diseases of tissue-resident macrophages. *Nature*. 2023;618(7966):698-707. doi:<https://doi.org/10.1038/s41586-023-06002-x>
10. Uderhardt S, Martins AJ, Tsang JS, Lämmermann T, Germain RN. Resident Macrophages Cloak Tissue Microlesions to Prevent Neutrophil-Driven Inflammatory Damage. *Cell*. 2019;177(3):541-555.e17. doi:<https://doi.org/10.1016/j.cell.2019.02.028>
11. Meziani L, Mondini M, Petit B, et al. CSF1R inhibition prevents radiation pulmonary fibrosis by depletion of interstitial macrophages. *The European Respiratory Journal*. 2018;51(3):1702120. doi:<https://doi.org/10.1183/13993003.02120-2017>
12. Buechler MB, Fu W, Turley SJ. Fibroblast-macrophage reciprocal interactions in health, fibrosis, and cancer. *Immunity*. 2021;54(5):903-915. doi:<https://doi.org/10.1016/j.immuni.2021.04.021>

13. Ries CH, Hoves S, Cannarile MA, Rüttinger D. CSF-1/CSF-1R targeting agents in clinical development for cancer therapy. *Current Opinion in Pharmacology*. 2015;23:45-51. doi:<https://doi.org/10.1016/j.coph.2015.05.008>
14. Fujiwara T, Yakoub MA, Chandler A, et al. CSF1/CSF1R Signaling Inhibitor Pexidartinib (PLX3397) Reprograms Tumor-Associated Macrophages and Stimulates T-cell Infiltration in the Sarcoma Microenvironment. *Molecular Cancer Therapeutics*. 2021;20(8):1388-1399. doi:<https://doi.org/10.1158/1535-7163.mct-20-0591>
15. King NicholasJC, Spiteri A. Putting PLX5622 into perspective: microglia in central nervous system viral infection. *Neural Regeneration Research*. 2023;18(6):1269. doi:<https://doi.org/10.4103/1673-5374.360170>
16. Spangenberg E, Severson PL, Hohsfield LA, et al. Sustained microglial depletion with CSF1R inhibitor impairs parenchymal plaque development in an Alzheimer's disease model. *Nature Communications*. 2019;10(1). doi:<https://doi.org/10.1038/s41467-019-11674-z>
17. Cai H, Zhang Y, Wang J, Gu J. Defects in Macrophage Reprogramming in Cancer Therapy: The Negative Impact of PD-L1/PD-1. *Frontiers in Immunology*. 2021;12. doi:<https://doi.org/10.3389/fimmu.2021.690869>
18. Hume DA, MacDonald KPA. Therapeutic applications of macrophage colony-stimulating factor-1 (CSF-1) and antagonists of CSF-1 receptor (CSF-1R) signaling. *Blood*. 2011;119(8):1810-1820. doi:<https://doi.org/10.1182/blood-2011-09-379214>
19. Li Y, Zhang Y, Pan G, Xiang L, Luo D, Shao J. Occurrences and Functions of Ly6Chi and Ly6Clo Macrophages in Health and Disease. *Frontiers in Immunology*. 2022;13. doi:<https://doi.org/10.3389/fimmu.2022.901672>
20. Van Overmeire E, Stijlemans B, Heymann F, et al. M-CSF and GM-CSF Receptor Signaling Differentially Regulate Monocyte Maturation and Macrophage Polarization in the Tumor Microenvironment. *Cancer Research*. 2016;76(1):35-42. doi:<https://doi.org/10.1158/0008-5472.can-15-0869>
21. Babaeijandaghi F., Cheng R, Kajabadi N., et al. Metabolic reprogramming of skeletal muscle by resident macrophages points to CSF1R inhibitors as muscular dystrophy therapeutics. *Science Translational Medicine*. 2022;14(651). doi:<https://doi.org/10.1126/scitranslmed.abg7504>
22. Lendeckel U, Venz S, Wolke C. Macrophages: shapes and functions. *ChemTexts*. 2022;8(2). doi:<https://doi.org/10.1007/s40828-022-00163-4>
23. Castro B, Kuang S. Evaluation of Muscle Performance in Mice by Treadmill Exhaustion Test and Whole-limb Grip Strength Assay. *BIO-PROTOCOL*. 2017;7(8). doi:<https://doi.org/10.21769/bioprotoc.2237>
24. Brummer H, Zhang MY, Piddoubny M, Medler S. Hybrid Fibers Transform into Distinct Fiber Types in Maturing Mouse Muscles. *Cells Tissues Organs*. 2013;198(3):227-236. doi:<https://doi.org/10.1159/000355280>
25. Heezen LGM, Abdelaal T, van Putten M, Aartsma-Rus A, Mahfouz A, Spitali P. Spatial transcriptomics reveal markers of histopathological changes in Duchenne

- muscular dystrophy mouse models. *Nature Communications*. 2023;14:4909.  
doi:<https://doi.org/10.1038/s41467-023-40555-9>
26. Klemm F, Möckl A, Salamero-Boix A, et al. Compensatory CSF2-driven macrophage activation promotes adaptive resistance to CSF1R inhibition in breast-to-brain metastasis. *Nature Cancer*. 2021;2(10):1086-1101.  
doi:<https://doi.org/10.1038/s43018-021-00254-0>
  27. Girardi F, Taleb A, Ebrahimi M, et al. TGF $\beta$  signaling curbs cell fusion and muscle regeneration. *Nature Communications*. 2021;12(1).  
doi:<https://doi.org/10.1038/s41467-020-20289-8>
  28. Arnold L, Henry A, Poron F, et al. Inflammatory monocytes recruited after skeletal muscle injury switch into antiinflammatory macrophages to support myogenesis. *The Journal of experimental medicine*. 2007;204(5):1057-1069.  
doi:<https://doi.org/10.1084/jem.20070075>
  29. Lemos DR, Babaeijandaghi F, Low M, et al. Nilotinib reduces muscle fibrosis in chronic muscle injury by promoting TNF-mediated apoptosis of fibro/adipogenic progenitors. *Nature Medicine*. 2015;21(7):786-794.  
doi:<https://doi.org/10.1038/nm.3869>
  30. Mass E, Nimmerjahn F, Kierdorf K, Schlitzer A. Tissue-specific macrophages: how they develop and choreograph tissue biology. *Nature Reviews Immunology*. Published online March 15, 2023:1-17.  
doi:<https://doi.org/10.1038/s41577-023-00848-y>
  31. Kamalika Mojumdar, Liang F, Giordano C, et al. Inflammatory monocytes promote progression of Duchenne muscular dystrophy and can be therapeutically targeted via CCR 2. *EMBO*. 2014;6(11):1476-1492.  
doi:<https://doi.org/10.15252/emmm.201403967>
  32. Sali A, Gueron AD, Gordish-Dressman H, et al. Glucocorticoid-Treated Mice Are an Inappropriate Positive Control for Long-Term Preclinical Studies in the mdx Mouse. *PLoS ONE*. 2012;7(4). doi:<https://doi.org/10.1371/journal.pone.0034204>
  33. Robinson A, Han CZ, Glass CK, Pollard JW. Monocyte Regulation in Homeostasis and Malignancy. *Trends in Immunology*. 2021;42(2):104-119.  
doi:<https://doi.org/10.1016/j.it.2020.12.001>
  34. Huang X, Khoong Y, Han C, et al. Targeting Dermal Fibroblast Subtypes in Antifibrotic Therapy: Surface Marker as a Cellular Identity or a Functional Entity? *Frontiers in Physiology*. 2021;12. doi:<https://doi.org/10.3389/fphys.2021.694605>